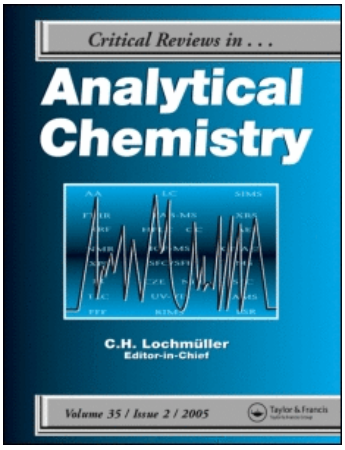

Critical Reviews in Analytical Chemistry
Publication details, including instructions for authors and subscription information:
http://www.informaworld.com/smpp/title~content=t713400837

Sub-Shot-Noise Light Sources: A Quiet Revolution in Light Control

Stephen E. Bialkowski[a]
[a] Department of Chemistry and Biochemistry, Utah State University, Logan, UT

To cite this Article Bialkowski, Stephen E.(1996) 'Sub-Shot-Noise Light Sources: A Quiet Revolution in Light Control', Critical Reviews in Analytical Chemistry, 26: 2, 101 — 147
To link to this Article: DOI: 10.1080/10408349608050569
URL: http://dx.doi.org/10.1080/10408349608050569

Critical Reviews in Analytical Chemistry, 26(2&3):101–147 (1996)

Sub-Shot-Noise Light Sources: A Quiet Revolution in Light Control

Stephen E. Bialkowski
Department of Chemistry and Biochemistry, Utah State University, Logan, UT 84322-0300

ABSTRACT: A review of current research trends in the control and measurement of the statistical properties of light is given. This review is limited to squeezing, sub-Poisson light, and methods for measuring properties of the resulting stabilized light. Basic descriptions of the statistical properties of light, electronic noise, and behavior are given. The results are used to illustrate how the unique properties of these optical sources and detection techniques may be used to improve the precision of the analytical measurement.

KEY WORDS: squeezed light, sub-poisson light, photon statistics, optical noise, optical spectroscopy.

I. INTRODUCTION

The precision of an optical transmission measurement has long been considered to be shot noise limited. In the shot noise limit, the photon counting statistics are described by the Poisson distribution. In particular, the signal to noise ratio is equal to the square root of the average photon number. The theoretical shot noise limit can only be attained using ideal coherent excitation sources. Real laser sources are often far from ideal and exhibit chaotic $1/f$ or flicker noise and amplified stimulated emission noise. Both of these noise sources have photon statistics that deviate from the ideal Poisson distribution. On the other hand, significant progress has been made in stabilizing the chaotic behavior in coherent light sources. In addition, new detectors and detection schemes for utilization of this stabile radiation have been described. In fact, it is now possible to generate and detect light with precision greater than that of the shot noise limit.

This article is for the analytical spectroscopist. It is intended to describe some basic concepts and recent results of electro-optics as they apply to optical measurement science. In particular, the basic principles of squeezed states and the art in generating sub-Poisson, squeezed states of light are discussed. A minimum theoretical framework is given to aid in an understanding of the special properties of this light. Literature regarding optical statistics and nonlinear control is dense. For example, a "noise with optical" key word search on one engineering literature data base returned over 10,000 citations from 1985 to 1995. However, most of this literature deals with noise reduction for specific cases or is theoretical in nature. Moreover, the increased accessibility and usability of literature on computer databases, and new CD ROM collections reduce the need for comprehensive literature reviews. Only key articles are referenced in this review article. Review articles and books are given where possible.

1040-8347/96/$.50

II. HISTORIC BACKGROUND

There has been steady progress in understanding light properties since Einstein reported the distribution for black-body radiation in 1909 and introduced the dilemma of particle-wave duality through the energy fluctuation equation.[1] The theory basis was advanced with the advent of quantum mechanical models and the electronic measurement techniques of the 1950s.[2] The statistical nature of both chaotic thermal and laser light, as related to the uncertainty principle and coherence were understood by 1965.[3] Coherence and the interaction of light and matter manifested in the observation that the coherent quantum states of light and matter are inseparable.[4] Concepts of coherent states of matter and electromagnetic radiation are now common, for example, in the operational principles of Fourier transform NMR. Many books now address the topic of optical spectroscopy based on the common coherence of matter and light.[5,6] Although this approach to optical spectroscopy is technically more difficult than the isolated molecule picture we prefer to use, the implications of this approach are comprehensible and more complete. The implication of this model to chemical analysis is clear. The measurement statistics, such as mean and variance, are related to those of the light and the way that the light interacts with the sample. There are few examples of applications of the quantum models for coherence spectroscopy measurement statistics to understanding the parameters such as limits of detection, etc. in chemical analysis. Statistics for multiphoton absorption, Raman, stimulated Raman, and four wave mixing, among other cases, have been worked out from a fundamental standpoint.[5–7]

Recently, significant advances in understanding control of the measured statistics havetaken place. Nature yields states of light with measurable values that are limited by the uncertainty principle. Measured values, for example, optical field photon number and phase, and the fluctuations of these values can be described by quantum mechanics. Measurements may be described by the expectation values of quantum mechanics operators and the fluctuations by commutation of the operators describing related measurements. Non-zero commutation values are a manifestation of the uncertainty principle. Some measurement statistics may be obtained from operator expectations and the commutation of the related operators. The expectation is the mean value and the fluctuation, or variance, in the related measurements are obtained from both operator commutation and standard formulas relating the measurement to the statistical variance. This quantum mechanical approach to measurement statistics is strictly valid for single optical mode, coherent states, and may be extended to incoherent or thermal states by stochastic superposition of several coherent modes.[3,8]

III. PHOTON STATISTICS

There are two main measurement techniques used to characterize statistics of optical radiation. The first is through field magnitude measurements. Field magnitude measurement are made by using interferometric homodyne detection.[6] This technique is important when examining phase-dependent statistics. The second technique is to measure photon number and its variance or the complete probability density.[8] This is performed by direct photon count or detector current measurement. Classic coherent optical states yield photon number measurement statistics that are Poisson distributed. The Poisson particle count distribution gives rise to the shot noise limit. However, the uncertainty in field amplitudes of different coherent modes are equal and limited by that allowed by the uncertainty principle. Different optical states can be generated wherein the field uncertainties of one component of

the wave (e.g., phase or amplitude) are less than that minimum allowed by the uncertainty principle for coherent states. These "minimum-uncertainty" states can have photon number distributions with variances less than that of the Poisson. These "sub-Poisson" states are nonclassic in that they do not result from the usual coherent states. These are squeezed states. A good overview of the development of nonclassic states derived from coherent states is given in Peřina's collection.[7] Teich and Saleh give a general development of sub-Poisson and anti-bunched states that includes chaotic and thermal sources.[9]

A few minimum-uncertainty states have received most of the attention because of their potential applications in optical communications and measurement sciences. The first is quadrature phase squeezed light in which the uncertainty in the phase of one of two quadrature components of the electromagnetic field amplitude, $\Delta\hat{a}_1$, is reduced at the cost of increasing the uncertainty of the other, $\Delta\hat{a}_2$. These two quadrature components are the sine and cosine terms of the electromagnetic wave. The uncertainty principle applied to the fluctuations of the two quadrature terms results in $\sigma_1^2\sigma_2^2 \geq 1/16$, where σ_i are the variances of the $\hat{a}_i$ quadrature phase, $\sigma_i^2 = \langle\langle(\hat{a}_i - \langle\hat{a}_i\rangle)^2\rangle = \langle\langle(\Delta\hat{a}_i)^2\rangle$, and the angle brackets indicate the expectation. A stabilized single-mode laser can operate at the "vacuum" fluctuation limit, wherein the equality holds in the uncertainty expression. With equal fluctuations in the two quadratures, $\sigma_1^2 = \sigma_2^2 = 1/4$. This uncertainty is called the "vacuum" limit because uncertainty in the quadrature phases is true also for the ground or vacuum state. Phase sensitive homodyne or heterodyne detection can be used to measure phase shifts to a precision that is better than that which could be obtained with a classic state of light.[10,11] This effect could have important implications in chemical analysis based on interferometric phase shift response. One such application is photothermal interferometry. There have been many technical improvements resulting in the generation and measurement of light in these states.

Another nonclassic state of interest is that of anti-bunched light. Photon bunching is a time or space correlated photon coincidence event. It can be described by a second order, that is, squared field or intensity, correlation function

$$g^{(2)}(\tau) = \frac{\langle\Phi(t)\Phi(t-\tau)\rangle}{\langle\Phi(t)\rangle\langle\Phi(t-\tau)\rangle} \qquad (1)$$

where $\Phi(t)$ is intensity or power at time t. A similar second-order correlation exists for space, $g^{(2)}(\rho)$, where ρ is a spatial coordinate. For coherent sources, $g^{(2)}(\tau) = 1$, that is, there is no correlation between photons or photon detection events. Anti-bunched light is that which has reduced correlations at or near $\tau = 0$.[9,12] The importance of this may not be immediately apparent. However, thermal sources exhibit $g^{(2)}(0) \geq 1$. Correlations between photons produced from thermal sources was first observed in 1956 by R. Hanbury Brown and R. Q. Twiss[13] by the spatial correlation of photon detection events. They used a 50% beamsplitter to separate the light from a Hg lamp into two beams from which they could measure spatial correlations. They found a significant deviation from $g^{(2)}(\rho) = 1$ in that $g^{(2)}(0) > 1$. Their later analysis revealed that the correlated photon events arise due to wave nature of electromagnetic radiation and they coined the term "wave interaction" noise.[14,15]

Hanbury Brown and Twiss observed the bunching effect in spatial correlation. That bunching also occurs in time was confirmed by Morgan and Mandel.[16] The bunching effect can also be found in the 1909 Einstein work that showed, in essence, that the fluctuation in the number of photons, n, was $\sigma_n^2 = \langle n\rangle + \langle n\rangle^2$. The first term part of this photon number variance expression is due to

the particle nature of light (i.e., the photon) and gives rise to shot-noise in the optical detectors. The second term, that proportional to the square photon count, is due to the "wave interaction" noise of Hanbury Brown and Twiss.[14] This discovery launched the scientific endeavor wherein experimental observations were reconciled within the theoretical basis of the statistical properties of light.

It is known that the first term in the photon variance gives rise to the usual Poisson probability density function (PDF)[8,17]

$$P(n) = \frac{\langle n \rangle^n}{n!} e^{-\langle n \rangle} \tag{2}$$

Here the PDF is written in terms of the number expectation or mean, $\langle n \rangle$, to avoid excessive parameter definitions. Typically, the PDF expectation is equal to a parameter, a, of the parent population. The number expectation operation results in $\langle n \rangle = a$. More fundamentally, the parent population parameter is $a = kp$, where k is the number of sampled volumes or cells, and p ($0 \le p \le 1$) is the probability of measuring an event, such as photon detection, within each sampled volume. This parameter can also be cast in terms of time parameters because photon production is a rate process. In this case k is replaced by the measurement time, t (s), and p by the generation rate, r (s^{-1}). Photon detection experiments that yield Poisson PDF are called shot-noise-limited.

The second term, observable for thermal sources and for short times, small volumes, and optical frequency intervals, and with photon high number densities,[2,3] gives rise to quite a different photon count distribution. In this case the variance is equal to the squared average photon number. In analytical spectroscopy, we would say that the signal to noise ratio (SNR) would be unity in this case. The Bose-Einstein distribution

$$P(n) = \frac{\langle n \rangle^n}{(1+\langle n \rangle)^{n+1}} \tag{3}$$

gives both limiting results. With low photon numbers in the oscillator modes, the Bose-Einstein distribution appears to be Poisson. With higher photon mode occupation, thermal radiation produces an exponential distribution, $P(\Phi,\langle\Phi\rangle) = \langle\Phi\rangle^{-1} \exp(-\Phi/\langle\Phi\rangle)$, per emission direction. With ensemble averaging over polarization and space, the total PDF is $P(\Phi,\langle\Phi\rangle) = 4\Phi\langle\Phi\rangle^{-2} \exp(-2\Phi/\langle\Phi\rangle)$.[8] The later black-body radiation probability density has a mean of $\langle\Phi\rangle$ and a variance of $\sigma_\Phi^2 = 1/2\langle\Phi\rangle^2$. The intensity proportional character of the standard deviation is indicative of source flicker noise wherein the noise or standard deviation is proportional to the intensity itself.

The photon number PDF can be used to obtain the expected mean and variance of the number count distribution using standard methods[17]

$$\langle n \rangle = \sum_{n=0}^{\infty} nP(n) \tag{4}$$

for the mean and

$$\sigma_n^2 = \langle n^2 \rangle - \langle n \rangle^2 = \sum_{n=0}^{\infty} n^2 P(n) - \left(\sum_{n=0}^{\infty} nP(n) \right)^2 \tag{5}$$

is used to obtain the variance. For short counting times, the mean and variance may be related to the second-order coherence function through

$$g^{(2)}(0) = \frac{\sigma_n^2}{\langle n \rangle^2} + 1 \tag{6}$$

Lasers produce Poisson distributed light even though the radiation is of small volume and optical frequency intervals, and the pho-

ton number densities are high. In fact, what analytical spectroscopists have come to believe is normal Poisson distributions giving rise to shot noise limited detection is not produced by classic thermal sources, but rather by coherent laser sources.

The Bose-Einstein distribution arises from thermal equilibration between the field and the emitters. The Poisson is found to be more appropriate for describing the statistics of coherent states generated by lasers, which becomes more apparent in the discussions of coherent states below. However, amplified spontaneous emission of a laser can be source of bunched thermal photons. The photon probability of this emission closely follows the Bose-Einstein distribution.[18] Thermal sources in which small phase volumes are sampled, for example, narrow spectral bandwidth lamps, as in the Hanbury Brown and Twiss experiments, will exhibit Bose-Einstein distributed light. The effects of classic Bose-Einstein light on optical absorption experiments has not concerned analytical spectroscopists in the past. This is because the thermal sources used were of extended area and interferometer and spectrometers were of limited wavelength resolution (see, for example, Teich and Saleh[9] or Mandel and Wolf[8]). The underlying exponential PDF is not normally observed in thermal sources used in spectrophotometry. This is due to several factors. First, conventional sources are spatially larger than that of single mode radiation. The superposition of Bose-Einstein emitters produced by a spectrally and spatially broad source result in a photon number distribution that is essentially Poisson, an effect of the central limit theorem.[17] Mandel and Wolf show that the photon number variance is $\sigma_n^2 = \langle n \rangle + \langle n \rangle^2/\mu$, where μ is the number of modes equal to the measurement to coherence time ratio.[8] Second, the spectral bandwidth is broad and the light is not polarized. The coherence time is equal to the inverse spectral bandwidth, $\Delta\nu$, for thermal sources. Third, the average mode occupation number, $\langle n_\nu \rangle = (e^{h\nu/kT}-1)^{-1}$, is much less than one in the visible ultraviolet for incandescent thermal sources ($T \sim 3000$ K). Thus, $\sigma_n^2 = \langle n \rangle + \langle n \rangle^2/\mu \sim \langle n \rangle$ should hold for sufficiently long photon counting times. The average mode occupancy is higher in the mid-infrared. For example, the 10-μm photon occupancy is 1.62 for a 3000 K source and the photon number variance is $\sigma_n^2 \sim \langle n \rangle^2/\mu$ for unit μ. The change in the photon number probability distribution with volume of a Bose-Einstein state has been experimentally confirmed.[19]

Nonetheless, there is, a cautionary lesson within the phase space volume effects of thermal sources described by Bose-Einstein photon statistics. With the decreasing phase volumes of micro analysis, as when using optical fibers, and with the increasing spectral resolution of modern grating and interferometric instruments, we may soon have to determine whether the measurements we are making with conventional thermal sources are truly shot-noise-limited. The way out of this trap is through anti-bunching the thermal light source. Anti-bunched light can be obtained by selective deletion of correlated photon events, for example, through a simultaneous multiphoton absorption process. In this case, the proportional noise term in the Bose-Einstein variance should be reduced and the resulting radiation may be Poisson with a photon number variance $\sigma_n^2 = \langle n \rangle$ and a second order correlation of $g^{(2)}(0) = 1$. Anti-bunched states should be able to be obtained from both thermal and laser sources.

Thermal, Bose-Einstein distributed, and coherent, Poisson distributed states of light are the normal or classic states. Nonclassical states can be obtained by appropriately altering the light through interactions with matter, or, in some cases, by using space-charge limiting effects in charged species, in particular, electrons. Nonclassical states of light can be described through the second-order correlation function. Extending the $g^{(2)}$ reduction concept can result in sub-Poisson

light. With sub-Poisson states, the variance is less than that of the Poisson distribution, $\sigma_n^2 < \langle n \rangle$. In this case, the second-order coherence is less than one near zero, $g^{(2)}(0) < 1$. The state of the optical field that produces this sub-shot-noise light is referred to as a number density squeezed state. In the quadrature picture, these states are possible by amplifying the phase variance. The uncertainty relationship is still valid and a minimum-uncertainty state exists. Although the state of the art of these techniques is far from perfect, there are now several methods and devices that have been shown to produce number squeezed light.[1-3] None of these have been applied to analytical spectroscopy to my knowledge. Most recently, realization of apparent sub-Poisson states using incoherent light emitting diode (LED) sources have been reported with increasing frequency. As with thermal light sources, it is difficult to describe the photon states using the quantum mechanical model. Instead, characterization of these are performed by direct measurement of the PDF. One may be reminded that the Hanbury Brown and Twiss correlation results were reported before a theory was developed to describe the effect. However, although sub-Poisson emission in LED sources have not been adequately described theoretically, they were predicted by Teich and Saleh.[9]

IV. COHERENT STATES

A. Quantum Description

Coherent states are used to describe the properties of an ideal laser source. A coherent state is described for a single mode of the laser radiation. Each single mode has infinitesimally narrow band width and is of a given phase. Finite band width laser output can be described as a collection of single modes. The summary given here is based on the classic paper by R. J. Glauber[20] and has been used extensively to describe states of light.[2,7,8]

An electromagnetic field can be represented by a set of states, $|n_k\rangle$, in mode k, of angular frequency ω_k. The Hamiltonian may be represented by photon creation, $\hat{a}_k^\dagger$, and annihilation, $\hat{a}_k$, operators

$$H = \frac{1}{2}\sum_k \hbar\omega_k\left(\hat{a}_k^\dagger\hat{a}_k + \hat{a}_k\hat{a}_k^\dagger\right) \quad (7)$$

These operators have the commutation relation

$$\left[\hat{a}_k, \hat{a}_{k'}^\dagger\right] = \delta_{k,k'}$$
$$\left[\hat{a}_k^\dagger, \hat{a}_{k'}^\dagger\right] = \left[\hat{a}_k, \hat{a}_{k'}\right] = 0 \quad (8)$$

where k and k' are the indices of two modes and the delta function $\delta_{k,k'} = 1$ only if $k = k'$, that is, for a single mode. The modes are independent, as specified by the delta function behavior of the creation and annihilation operator commutation. The Hamiltonian for a single mode has eigenvalues, $\hbar\omega_k(n_k + 1/2)$. Thus, n_k an integer quantum number representing the occupancy level or number of photons in the mode. The $\hat{a}_k^\dagger$ and $\hat{a}_k$ operate on the $|n_k\rangle$ eigenstates to raise or lower the number of photon in the mode

$$\hat{a}_k|n_k\rangle = n_k^{1/2}|n_k - 1\rangle$$
$$\hat{a}_k^\dagger|n_k\rangle = (n_k + 1)^{1/2}|n_k + 1\rangle \quad (9)$$
$$\hat{a}_k^\dagger\hat{a}_k|n_k\rangle = n_k|n_k\rangle$$

These fundamental photon states are not convenient for describing the fields. Glauber introduced "coherent states", commonly referred to as in Glauber states,[2,7] to describe the electromagnetic radiation obtained from single mode sources such as the laser. The Glauber coherent state definition and mathematics associated with the theory was a turning point in quantum optics. Expansion in terms of the coherent states produced a mathematical frame work that was relatively

easy to work with and to extend to many measurement situations. The theory allowed relatively easy prediction of experimental observables, different photon states, and the experimental observables of these states. A brief summary of this theory is given here and some examples of observables are described below.

The coherent state, $|\alpha\rangle$, with a complex amplitude α is defined as an eigenstate of $\hat{a}$

$$\hat{a}|\alpha\rangle = \alpha|\alpha\rangle \tag{10}$$

The eigenstates are found from expansion of the $|n\rangle$ photon states

$$|\alpha\rangle = \sum_n |n\rangle\langle n|\alpha\rangle \tag{11}$$

Expansion coefficients are found from the recursion relationship between the photon and coherent states and by choosing the phase of the coherent state such that $\langle\alpha|\alpha\rangle = 1$. The coherent states are found to be

$$|\alpha\rangle = e^{1/2|\alpha|^2} \sum_n \frac{\alpha^n}{(n!)^{1/2}}|n\rangle$$

$$|\alpha\rangle = e^{-1/2|\alpha|^2} \sum_n \frac{(\alpha^*)^n}{(n!)^{1/2}}|n\rangle \tag{12}$$

The average occupancy number is the Poisson distribution

$$|\langle n|\alpha\rangle|^2 = \frac{\left(|\alpha|^2\right)^n e^{-|\alpha|^2}}{n!} \tag{13}$$

with mean, $\langle n\rangle$, and variance, σ_n^2 equal to $\alpha^*\alpha$. This also shows that the coherent state with eigenvalue, $\alpha = 0$, is the ground state $|n\rangle$ with $n = 0$. We take these coherent states as being appropriate representations of the field from a coherent source because of the appealing attributes that (1) the photon number is that observed for single mode sources and (2) the average photon occupancy in the mode is proportional to the square of the coherent field.

The coherent states are not orthogonal but can nonetheless be used as a basis to describe other coherent states. A density operator can be formulated

$$\rho = \int P(\alpha)|\alpha\rangle\langle\alpha|\, d^2\alpha \tag{14}$$

where $d^2\alpha$ is used to indicate integration over the real and imaginary parts of α. For a pure state, $\rho = |\alpha\rangle\langle\alpha|$. This functional definition of the density matrix, ρ, is commonly referred to as the Glauber-Sudarshan P distribution[11] because Sudarshan independently arrived at the same result.[21] Some characteristics of the density matrix are that it is Hermitian, has nonnegative eigenvalues, can be used to find the mean value of an operator through the trace of the product $Tr\{\rho A\} = \langle A\rangle$, and it has unit trace, $Tr\{\rho\} = 1$. Inasmuch as the coherent states are normalized (by choice of phase),

$$Tr\{\rho\} = \int P(\alpha)\, d^2\alpha = 1 \tag{15}$$

Thus, the $P(\alpha)$ term is similar to a probability density for the coherent states. The probability density function for the photon number occupancy can be found from $\langle n|\rho|n\rangle$, which is, of course, Poisson for pure coherent states. On the other hand, the density matrix is used to determine moments of the probability distribution. For example, the mean photon number is found from $Tr\{\rho\hat{a}^\dagger\hat{a}\}$. Glauber shows that higher orders of the photon number distribution, $\langle n^2\rangle$, $\langle n^3\rangle$, may be obtained if the creation and annihilation operators are ordered

$$Tr\left\{\rho\hat{a}^{\dagger n}\hat{a}^m\right\} = \int \alpha^{*n}\alpha^m P(\alpha)\, d^2\alpha \tag{16}$$

Any combination of creation and annihilation operators may be ordered in this fashion using the commutation relationship. For example, the photon number variance, $\sigma_n^2 = Tr\{\rho(\hat{a}^\dagger\hat{a} - Tr\{\rho\hat{a}^\dagger\hat{a}\})^2\}$ for a single coherent

state can be shown to be $\sigma_n^2 = Tr\{\rho\hat{a}^\dagger\hat{a}\} = \langle n\rangle = \alpha^*\alpha$. The correlation functions may also be determined from the density matrix. In the important case of the second-order correlation function

$$g^{(2)}(0) = \frac{Tr\left\{\rho\hat{a}^{\dagger 2}\hat{a}^2\right\}}{Tr\left\{\rho\hat{a}^\dagger\hat{a}\right\}^2} \qquad (17)$$

The second-order coherence function for a coherent state is unity, as expected for coherent radiation.

The density matrix may serve to connect the quantum description and the measurement statistics. Several examples of how the density matrix may be used to obtain photon statistics for coherent states have been shown.[2,7,21–25] Particularly appealing properties is that the Bose-Einstein distribution can be obtained and the form of $P(\alpha)$ for multiple modes is factorized, implying that the total probability is a product of the individual probabilities, as expected from fundamental measurement statistics.[17] Still, a problem exists in the density matrix for this basis. Because coherent states are not orthogonal, different linear combinations of coherent states may be used to describe a single elementary photon number distribution. Thus, $P(\alpha)$ may be singular for certain photon states.

These states specifically describe light within a cavity. For example, the description is valid for stationary modes within a laser oscillator and the α are the eigenvalues of the wave functions within this closed system. Similarly, the photon number, or its distribution, is that of the cavity modes. These parameters are also directly related to those measured from a dissipative system. In particular, cavity mode photon number statistics for a coherent state are the same as those of the field produced by the laser. The connection must be made with some care. The output coupler releases photons at a rate proportional to the pumping rate by random removal of photons from the cavity. Subsequently, the measured photon count statistics will change by the random removal (Bernoulli deletion[9]) process applied to the cavity photon statistics. Unbiased photon extraction at the output coupler is technically a binomial rate process. With low transmission output couplers, the Poisson theorem applies, and removal is a Poisson rate process. Subsequently, any cavity photon number distribution will result in a superposition of Poisson rate processes. With the Poisson photon number distributed coherent cavity states of a laser, the Poisson removal rate process results in another Poisson process with α^2 replaced by $\alpha^2 rt$, where r is the removal rate and t is the measurement time. Essentially, this is because the product of two random processes is represented by their convolution and the convolution of two Poisson processes is itself a Poisson process.[17] It is also worth noting that even if the photon number states are squeezed in the respect that only one state is occupied within the cavity, the Poisson random removal rate process will result in a Poisson distribution outside the cavity if the removal rate is sufficiently low.

B. Quadrature Components

The coherent states are eigenstates of the annihilation operator. Photon state creation and annihilation operators are not Hermitian and do not correspond to physically observed quantities. Hermitian operators may be obtained by linear combination of the photon state operators[7,22]

$$\hat{a} = a_i + i\hat{a}_2 \qquad (18)$$

where $\hat{a}_1$ and $\hat{a}_2$ are related to the position and momentum operators[25] and have the commutation relationship

$$\left[\hat{a}_i, \hat{a}_2\right] = \frac{i}{2} \qquad (19)$$

It follows that the eigenvalues or states of the Glauber coherent functions may be decomposed into corresponding components, $\alpha = \alpha_1 + i\alpha_2$, such that $\hat{a}_{1,2}|\alpha_{1,2}\rangle = \alpha_{1,2}|\alpha_{1,2}\rangle$.

The physical significance of the operators may be found by examining the electric field. The electric field, $\boldsymbol{E}(r,t)$, of a single mode coherent state can be expressed in terms of the photon operators[6,11]

$$\boldsymbol{E}(r,t) = \gamma(r)\left(\hat{a}e^{-i\omega t} - \hat{a}^{\dagger}e^{i\omega t}\right) \quad (20)$$

where $\gamma(r)$ is the space-dependent term $i(\hbar\omega/2\varepsilon)^{1/2}\boldsymbol{E}(r)$. Expressing the electric field in terms of $\hat{a}_1$ and $\hat{a}_2$

$$\boldsymbol{E}(r,t) = \frac{\gamma(r)}{2}\left(\hat{a}_1 \cos\omega t + \hat{a}_2 \sin\omega t\right) \quad (21)$$

Clearly, $\hat{a}_1$ and $\hat{a}_2$ have eigenvalues that are amplitudes of the sine and cosine quadrature components of the electric field. These field quadrature components are orthogonal. It is interesting that this equation also represents a state of a harmonic oscillator.[26] With this model, $\hat{a}_1$ would be the position operator and $\hat{a}_2$ that for the momentum. Position and momentum do not commute and the uncertainty principle states that the state of each cannot be simultaneously known to high precision.

The variances in the quadrature components are found using $\alpha_{1,2}^2 = \alpha\langle(\hat{a}_{1,2} - \langle\hat{a}_{1,2}\rangle)^2\rangle = \langle\Delta\hat{a}_{1,2}^2\rangle$, where the $\langle\hat{a}_{1,2}\rangle$ are used to indicate the trace density matrix operation, $Tr\{\rho\hat{a}_{1,2}\}$. The variances of the two quadratures are equal with

$$\langle\Delta\hat{a}_1^2\rangle = \langle\Delta\hat{a}_2^2\rangle = \frac{1}{4} \quad (22)$$

The uncertainty principle relationship is

$$\langle\Delta\hat{a}_1^2\rangle = \langle\Delta\hat{a}_2^2\rangle \geq \frac{1}{16} \quad (23)$$

Thus, the coherent states are minimum-uncertainty states in the sense that they have uncertainties that are the minimum allowed by the uncertainty principle. These states may be more clearly understood by their graphic representation. A convenient coordinate system is one where the two orthogonal axes are the sine and cosine field quadrature components. The center of the state is the eigenvalue α, at the coordinates (α_1,α_2). The distance to the center of the state is $|\alpha|$. The phase of the field is represented by angle that eigenvalue vector makes with the real axis. Interestingly, the variance of the eigenvalues (α_1,α_2) do not change with $|\alpha|$, that is, it is invariant to the displacement operation. This should not be confused with the photon number variance, which does change with $|\alpha|$.

V. QUADRATURE SQUEEZED STATES

A. Quantum Description

Quadrature squeezed states occur when the quadrature variances are unequally partitioned while still maintaining a product minimum-uncertainty state.[10,11] In other words, the quadrature variance product is 1/16, but the variances are not both equal to 1/4. In this case the phase variance of one quadrature is less than that of the other and less than that of the coherent state. This is illustrated in Figure 1. In the first part, **A** represents a coherent state with equal variance in both quadratures. Two quadrature amplitude variance squeezed states are represented in parts **B** and **C**. Part **B** represents a state where the amplitude variance is less for the high-amplitude quadrature component. This can result in a photon number variance less than that produced by coherent light. In Part **C**, the amplitude variance is less for the low-amplitude component. This type of squeezing, or anti-squeezing, produces a state with higher photon number variance. A theory that describes the relationship between the amplitude squeezed (or

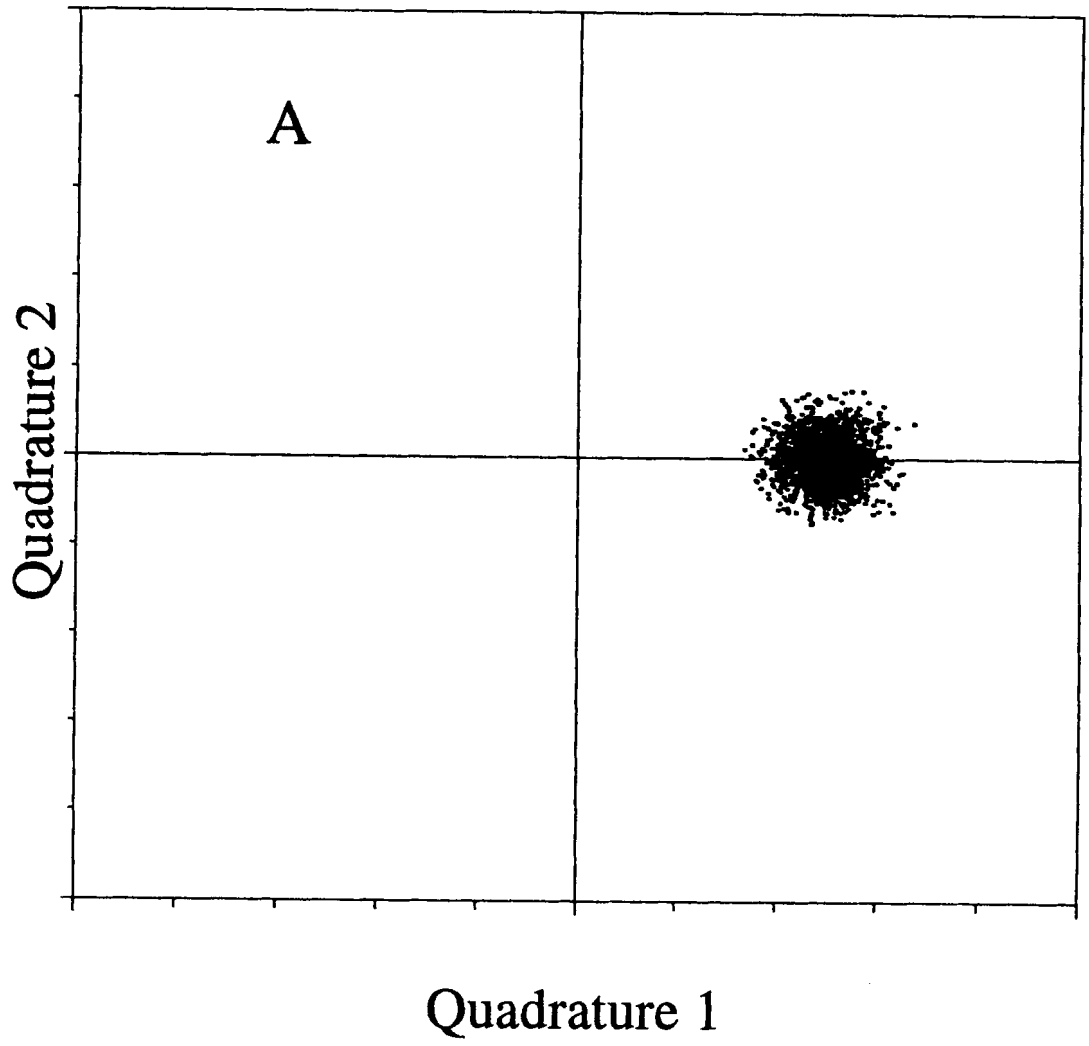

FIGURE 1. Probability density plots of (A) coherent state; (B) and (C) quadrature squeezed states. The two quadrature components make up the axes. The probability plots shown with scattered points indicate the range of field amplitude measurements. The vector distance to the center of the field amplitude probability is the proportional to photon number or optical power. The direction of this vector indicates the principle quadrature. Quadrature squeezing as in part (B) decreases the variance in the field or power measurements. Squeezing as in part (C) increases the variance.

anti-squeezed) states is examined here. Experimental realizations of squeezed states and their measurement is discussed later.

In theory, quadrature squeezed states can be composed using either "two-photon coherent states"[25] or by using the "squeeze operator".[10,27,28] Two-photon coherent states are eigenstates of an operator composed of a linear combination of photon creation and annihilation operators

$$\hat{b} = u\hat{a} + v\hat{a}^{\dagger} \qquad (24)$$

where u and v are complex, under the constraint that, $[\hat{b},\hat{b}^{\dagger}] = 1$. These states may be created in a two-photon laser or in degenerate parametric amplification.[25] Similar to the Glauber coherent states, the eigenstates of the two-photon coherent states are defined by $\hat{b}|\beta\rangle = \beta|\beta\rangle$, and many operations, for example, displacement and density matrix construction, can be similarly defined. The operator may be expanded in the quadrature components, $\hat{b} = \hat{b}_1 + i\hat{b}_2$, as can eigenvalues of the two-photon coherent states, $\beta = \beta_1 +$

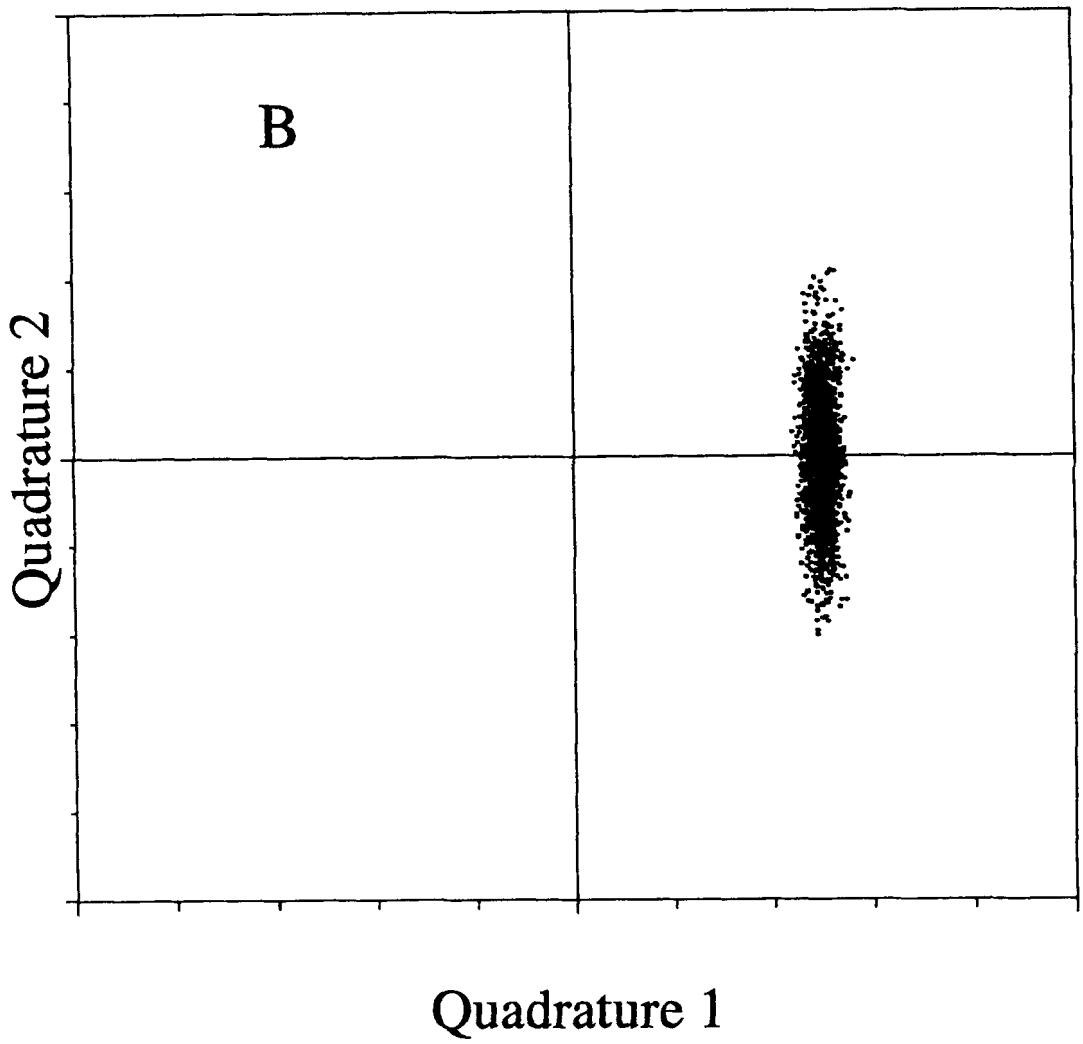

FIGURE 1B

$i\beta_2$. Because the electric field can be described in terms of the photon creation and annihilation operators, it may also be described in terms of the two-photon coherent state $\hat{b}$ operators.

One important difference between Glauber coherent states and the two-photon coherent states is that the uncertainty in the quadrature phase components are not necessarily equal or at the minimum allowed by the uncertainty principle. This can result in quadrature squeezed light. First, minimum-uncertainty states are produced when $u = \delta v$, where δ is a real number. The u and v parameters for general two-photon squeezed states may be expressed as[26]

$$u = \cosh r$$
$$v = ie^{i\theta} \sinh r \qquad (25)$$

where r is called the squeeze factor and θ is a phase that must meet certain criteria.[25] As discussed by Caves[10] and Walls,[11] quadrature squeezed two-photon states are Glauber states with eigenvalues rotated by $\theta/2$. The squeeze factor effectively attenuates one quadrature component of the eigenvalue while amplifying the other. Another difference is that although coherent states are generated with terms linear in creation and annihilation operators, the squeezed states are generated by quadratic terms. This fact turns

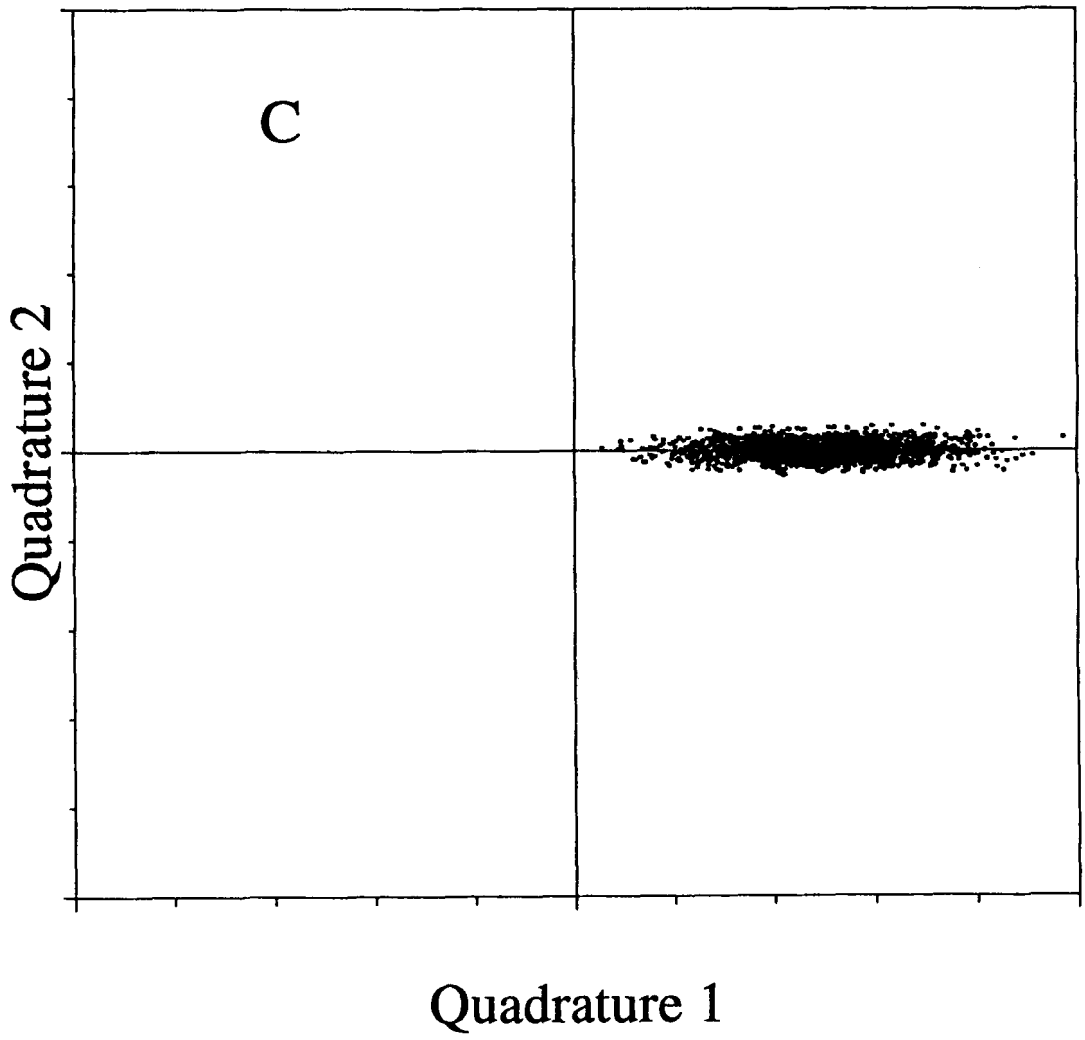

FIGURE 1C

out to be important in the quest for experimental realizations of quadrature squeezed light. Squeezing has been found in systems wherein the output can be described in terms of quadratic creation and annihilation operators.

The models predict that the quadrature variances are

$$\left\langle \Delta\hat{a}_1^2 \right\rangle = 1/4\, e^{-2r}$$

$$\left\langle \Delta\hat{a}_2^2 \right\rangle = 1/4\, e^{2r} \qquad (26)$$

As the absolute magnitude of the squeeze factor increases, the quadrature phase variance decreases in one component while increasing in the other. The r may be either positive or negative valued, representing squeezing of either the $\hat{a}_1$ or $\hat{a}_2$ quadrature component, respectively. Notice that the uncertainty principle is maintained as $\langle \Delta\hat{a}_1^2 \rangle \langle \Delta\hat{a}_2^2 \rangle = 1/16$. In fact, these are minimum-uncertainty states.

B. Photon Statistics

An interesting change occurs in the mean photon mode occupancy for the squeezed state

$$\langle n\rangle = \left|\hat{\beta}\right|^2 + |v|^2 = |\alpha|^2 + \sinh^2 r \quad (27)$$

where the right equation results from the rotation relationship between Glauber coherent states and minimum-uncertainty two-photon states[10]

$$\hat{\beta}_1 + i\hat{\beta}_2 = (\alpha_1 + i\alpha_2)e^{-i\theta/2} \quad (28)$$

That the mean number is not equal to the squared amplitude of the eigenvalue should not be too surprising given that the width of the α (or β) eigenvalue distribution is broadened due to distortion of the two-dimensional probability density. The $\sinh^2 r$ term in $\langle n\rangle$ represents the excess quantum noise of the squeezed vacuum state. The photon number variance in the squeezed state is calculated from $\sigma_n^2 = \langle \hat{a}^{\dagger 2}\hat{a}^2\rangle + \langle \hat{a}^\dagger \hat{a}\rangle - \langle \hat{a}^\dagger \hat{a}\rangle^2$, is[10,25]

$$\sigma_n^2 = \left(u^*\hat{\beta}^* - v^*\hat{\beta}\right)\left(u\hat{\beta} - v\hat{\beta}^*\right) + 2|v|^2\left(1+|v|^2\right)$$

$$\sigma_n^2 = \left|\alpha\cosh r - \alpha^* i e^{i\theta}\sinh r\right|^2 + 2\cosh^2 r\sinh^2 r \quad (29)$$

where $\langle \hat{a}^{\dagger 2}\hat{a}^2\rangle$ is determined using Yuen's Q matrix approach. The angle, θ, causes the α product to be real. Choosing a direction for α fixes θ for minimum-uncertainty states. The excess quantum noise in the vacuum squeezed state, that is, that with zero α, has a mean photon number of $\sinh^2 r$ and a photon number variance of 2 $\cosh^2 r$ $\sinh^2 r$. These may not be important from a practical standpoint. Typical values for $|r|$ are on the order of 1. In this case, the mean squeezed vacuum photon number is 1 and the standard deviation is 2.5. For cases where $|\alpha|^2 \gg \sinh^2 r$, $\langle n\rangle \sim |\alpha|^2$ and $\sigma_n^2 \sim |\alpha|^2 \exp(\theta 2r)$, for real α. It should be noted that r may be positive or negative valued. Thus, light with more than the shot-noise-limited variance may be produced.

A plot of the theoretical signal-to-noise ratio that would be obtained measuring squeezed light with a unit quantum efficiency detector is illustrated in Figure 2. The squeeze parameter increases from right to left and the number of photons increases moving from front to rear. The height of the surface is the SNR. As a reference, the line on the right edge of the surface corresponds to the usual shot noise limit wherein SNR = $\langle n\rangle^{1/2}$. The ridge corresponding to the maximum SNR occurs for a squeeze parameter of about 1.5 in this range. It is clear that quadrature squeezing significantly enhances the SNR in this range. Just as some squeezing can increase the SNR, too much squeezing will increase the variance through the hyperbolic terms. In this case the limiting signal to noise ratio, $\langle n\rangle/\sigma_n \sim 2^{-1/2}$, for $r \to \infty$. The minimum photon number variance is calculated to $\sigma_n^2 \approx \langle n\rangle^{2/3}$ for a quadrature squeezed state.[29]

The reason why the SNR decreases with r beyond optimum may be understood in terms of the quadrature distributions and the relationship between α and n. Without squeezing, the two quadrature components of α are normally distributed, with equal variance in both components. Because n is obtained from $|\alpha|^2 = \alpha_1^2 + \alpha_2^2$, we may consider that there are two components to the photon number variance; those due to α_1 and α_2 variances. From propagation of errors, $\sigma_n^2 = 4\alpha_1^2\sigma_{\alpha 2}^2 + 4\alpha_2^2\sigma_{\alpha 2}^2$. Minimum-uncertainty α states have $\sigma_{\alpha 1}$ and $\sigma_{\alpha 2}$ equal to 1/2. Thus, $\sigma_n^2 = \alpha_1^2 + \alpha_2^2 = |\alpha|^2 = \langle n\rangle$, as expected for a Poisson distribution. With reduced photon number fluctuation squeezing, the (α_1,α_2) distribution is narrower along one of the α axes and wider along the perpendicular axis. However, although the narrower α axis distribution decreases the photon number variance, say through the α_1^2 term, the wider α_2 distribution may increase the width of the α distribution (the photon number is proportional to the squared distance from the origin

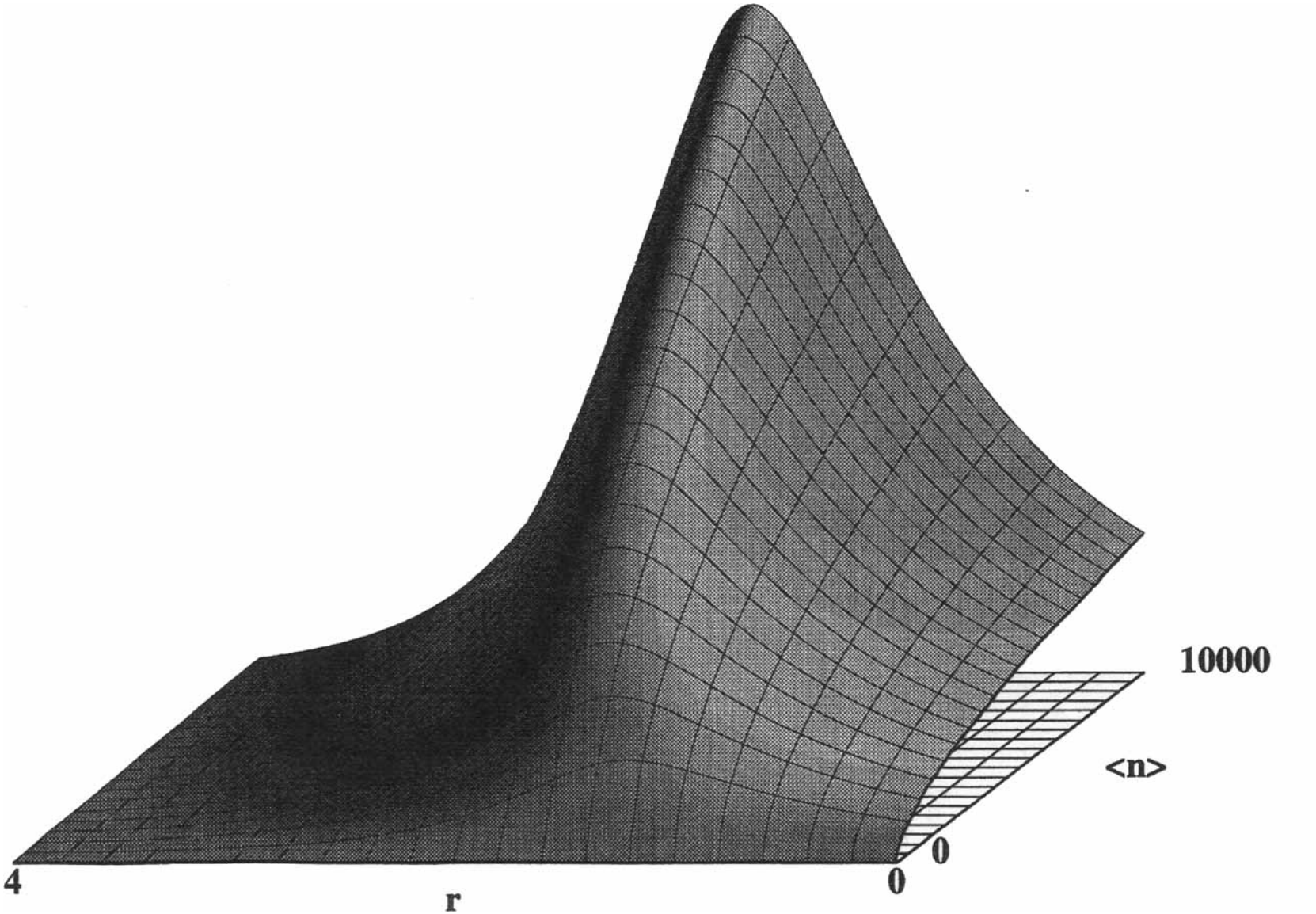

FIGURE 2. Signal-to-noise ratio with a unit quantum efficiency detector from quadrature squeezed states. The squeeze parameter, r, increases from right to left, the photon number expectation, $\langle n \rangle$ increases from front to rear. The relative signal-to-noise ratio is indicated by surface height

to the points in Figure 1). In this case, $\sigma_n^2 = \alpha_1^2 e^{-2r} + \alpha_2^2 e^{2r}$. Again, the increase in photon number variance is due to the increase in $|\alpha|$ variance that arises from distortion in the α distribution.

Some additional behavior of the photon statistics of squeezed light may be seen by examining the PDF. Yuen noted that the photon number of a two-photon coherent state was not Poisson, but rather[25]

$$\langle n|\beta\rangle = \left(\frac{1}{n!u}\right)^{1/2}\left(\frac{v}{2u}\right)^{n/2} H_n\left[\frac{u\hat{\beta}+v\hat{\beta}^*}{\sqrt{2uv}}\right] \exp\left(-\frac{1}{2}|\hat{\beta}|^2 - \frac{v}{2u}\hat{\beta}^{*2}\right) \quad (30)$$

where $H_n[z]$ is the nth Hermite polynomial of the complex argument, z. The PDF is the product with the complex conjugate. As above, the eigenvalues may be represented in terms of those of the $|\alpha\rangle$ for the correct rotation. In addition, because minimum-uncertainty states occur for $u/v = \delta$, with real δ, $v/u = \pm\tanh r$. Minimum-uncertainty two-photon coherent $\hat{a}_1$ quadrature squeezed states (i.e., real α) yield the photon number density[26,30]

$$P(n;\alpha,r) = \operatorname{sech} r e^{-\alpha^2(1+\tanh r)}\left(\frac{\tanh^n r}{2^n n!}\right) H_n^2\left[\frac{\alpha}{\sqrt{2}}\left(\tanh^{1/2} r + \coth^{1/2} r\right)\right] \quad (31)$$

This complex PDF indicates how quadrature squeezing will affect the "noise" in the measured photon number.

The photon number distribution is plotted in Figure 3 as a function of the squeeze parameter, r, from 0 to 2, and with real α of 5. The distribution is Poisson in the limit as $\tanh r \to 0$. The squeezed state reduced to a Glauber coherent state in this limit, that is, $v \to 0$. The Poisson distribution is observed at the front of the plot, $r = 0$. As r increases, indicating more quadrature squeezing, the PDF initially narrows, in the sense that the variance decreases. The most probable photon number also increases with increasing r. For larger amounts of squeezing the distribution broadens and becomes periodic. The oscillating photon number probability density has been described in terms of the asymmetric section that a quadrature squeeze state cuts through the phase space of the harmonic oscillator.[30] The normal concept of variance may not be meaningful for highly squeezed states at low photon number density. The point where the photon number distribution width is minimum yet there is no oscillation is for $r \sim 0.5$, in qualitative agreement with the estimate of $r \leq (2/3)\ln(9\pi\alpha/8)$ for no oscillation. Oscillation in number density does not occur for large α. Using the fact that $H_n[z] \approx (2z)^n$ for large z results in

$$P(n;\alpha \gg 1, r) \approx \operatorname{sech} r e^{-\alpha^2(1+\tanh r)} \frac{\left[\alpha^2(1+\tanh r)^2\right]}{n!} \quad (32)$$

This is similar to a Poisson distribution with $\langle n\rangle = \sigma_n^2 = [\alpha(1 + \tanh r)]^2$. The decrease in the theoretical SNR with greater than optimum squeeze parameters observed in the previous figure is then due to the broadening of the photon count distribution associated with high r and $|\alpha|^2$.

C. Second-Order Correlation and Anti-Bunching

As shown above, both quadrature and photon number squeezing can result in sub-Poisson light generation. The relationship between squeezing, anti-bunching, as predicted through second-order coherence, and sub-Poisson photon counting statistics has been described by several authors.[2,9,11,31–33] These states of light are not necessarily re-

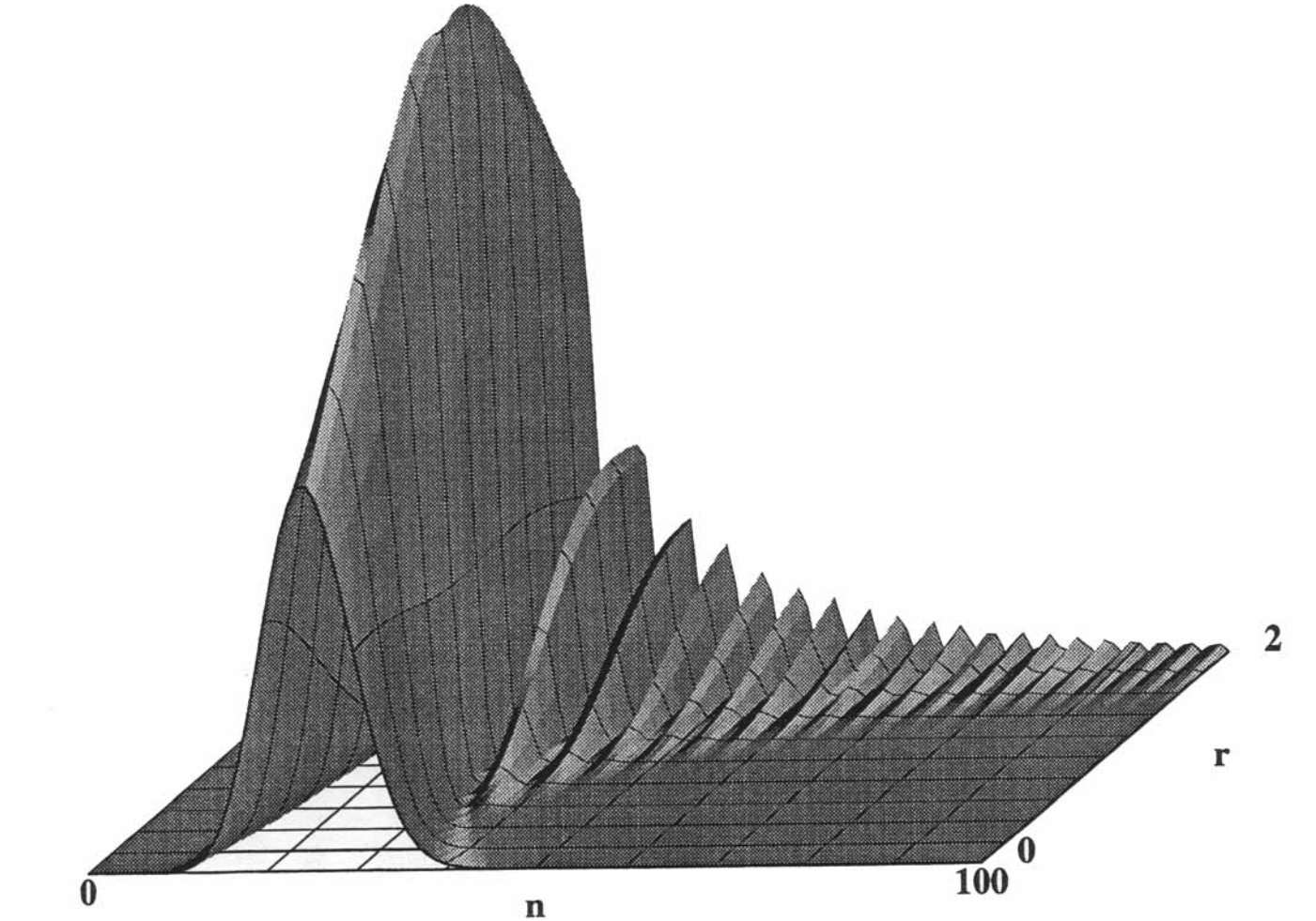

FIGURE 3. Probability density function for quadrature squeezed light as a function of the squeeze parameter, *r*. The photon number, *n*, distribution is Poisson for small *r*. The data were calculated using a real α of 5 and the corresponding average photon number is 25.

lated. The field correlation can be calculated to any order using $g^{(n)} = \langle \hat{a}^{\dagger n} \hat{a}^n \rangle / \langle \hat{a}^\dagger \hat{a} \rangle^n$. Photon anti-bunching, and bunching, is related to the second-order correlation $g^{(2)} = \langle \hat{a}^{\dagger 2} \hat{a}^2 \rangle / \langle \hat{a}^\dagger \hat{a} \rangle^2$. The latter can be evaluated in terms of the variance $\sigma_n^2 = \langle \hat{a}^{\dagger 2} \hat{a}^2 \rangle + \langle \hat{a}^\dagger \hat{a} \rangle - \langle \hat{a}^\dagger \hat{a} \rangle^2$, and mean photon number $\langle n \rangle = \langle \hat{a}^\dagger \hat{a} \rangle$,

$$g^{(2)}(0) = 1 + \frac{\sigma_n^2 - \langle n \rangle}{\langle n \rangle^2} \qquad (33)$$

With no squeezing, the variance and mean are equal and $g^{(2)} = 1$, indicative of a Poisson photon number count distribution. Sub-Poisson light occurs when the photons are anti-bunched.[9] An operational definition of "sub-Poisson" is a photon number count distribution wherein the mean number of photon counts is greater than the variance $\langle n \rangle > \sigma_n^2$. Anti-bunching occurs when the second-order coherence function is less than one, $g^{(2)} < 1$. For this to be true, $(\sigma_n^2 - \langle n \rangle) / \langle n \rangle^2 < 1$, which is the equivalent to the sub-Poisson condition $\langle n \rangle > \sigma_n^2$. Thus, anti-bunched light is sub-Poisson in the respect that the mean photon number is greater than the variance. For quadrature squeezed light, the condition for anti-bunching is $2\langle n \rangle > e^r \sinh r(2 \sinh 2r + 1)$. This condition can usually be met because of the positive exponential r dependence.

D. Quadrature Squeezed Light Production

The theory of quadrature squeezed light was developed long before the first experimental realizations. Several theoretical predictions were found to be true and theory guided the experimental aspects. Even the applications of squeezed light in communications[34] and optical measurements[10,11] were discussed and in some cases theoretically developed before the first realization. Walls[11] reviewed several predicted means of quadrature squeezing prior to the first successful experimental realization. Based on a straightforward interpretation of Yuen's two-photon coherent state operator, $b = u\hat{a} + v\hat{a}^\dagger$, Walls noted that mixing a coherent mode, $\hat{a}$, with its phase conjugate, $\hat{a}^\dagger$, such that $|u|^2 - |v|^2 = 1$ will produce these squeezed states. Subsequently, schemes based on optical phase conjugation through four-wave mixing interactions could produce quadrature squeezed light. This experimental proof came more than 10 years after the initial predictions of quadrature squeezed states. Two things happened in that 10-year period. First, the theory was examined by several authors who added thoughts toward experimental realizations. Second, the technology of coherent light generation and stabilization, as well as the means for detecting quadrature squeezed states, were developed.

In 1985, Reid and Walls[35] extended the theory of four-wave mixing and degenerate four-wave mixing for quadrature squeezing. The first experimental realization was obtained by Slusher et al.[36,37] later that year. The experiment used nondegenerate four-wave mixing with a cavity. The experimental apparatus was complicated, primarily owing to the fact that definitive detection of squeezed states requires a measurement standard at the shot noise limit. Sodium vapor was used as the nonlinear mixing medium. Squeezing was detected using a balanced detector system. The coherent excitation was mixed with the squeezed light produced by four-wave mixing within a cavity. A cavity was used to build up appreciable amounts of light in the squeezed state. Data analysis revealed a 0.3 dB noise suppression, or a 7% reduction in noise, corresponding to almost 20% squeezing of the cavity output.

Although a 0.3 dB noise reduction may not seem impressive in retrospect, it should be kept in mind that this was the first time that such a nonclassic state of light was observed. In addition, there was a lot of excess noise in these experiments that obscured the squeezed light measurements. These included

Johnson noise in the electronic circuitry and acoustic or phase noise due to small changes in optical pathlengths in the interferometers and the homodyne detector. The excess noise sources may be substantially reduced with current detector technology. additional, excess noise was attributed to spontaneous emission of the sodium vapor used as the active medium.

More insight into the potential means for squeezed light generation can be obtained by examining the quantum mechanical operators for field generation. The displacement operator for production of coherent states of light is linear in creation and annihilation operators.[2,7] For example, a coherent state, $|\alpha\rangle$, can be produced by displacement of a vacuum

$$|\alpha\rangle = D(\alpha)|0\rangle$$

$$D(\alpha) = \exp\left(-1/2\alpha^*\alpha - \alpha^*\hat{a} + \alpha\hat{a}^\dagger\right) \quad (34)$$

Quadrature squeezed states are similarly produced with a "squeeze operator"[10,11,25–28]

$$|\alpha,\zeta\rangle = D(\alpha)S(\zeta)|0\rangle$$

$$S(\zeta) = \exp\left(1/2\zeta^*\hat{a}^2 - 1/2\zeta\hat{a}^{\dagger 2}\right) \quad (35)$$

Thus, squeezed states result from second-order interactions of light because the squeeze operator uses quadratic creation and annihilation operators. Walls pointed out that a prototype interaction Hamiltonian for these second order interactions would be of the form

$$H = \hbar\left(\chi^{(n)} * E^{n-1}\hat{a}^2 + \chi^{(n)}E^{n-1}\hat{a}^{\dagger 2}\right) \quad (36)$$

where the $\chi^{(n)}$ are nth order optical susceptibilities and E is the field amplitude. Optical parametric amplification is described by this Hamiltonian with a $\chi^{(2)}$ process, whereas four-wave mixing is a $\chi^{(3)}$ process. The general form of the equation also allows for the possibility of squeezed state production by second harmonic generation, multiphoton absorption, and coherent Raman effects. (However, stimulated Raman light produced with coherent sources is super-Poisson with an exponential PDF[38–40].)

Wu et al. observed quadrature squeezed states with parametric down conversion in 1986.[41] The degree of squeezing was small but observable. Later Kimble, Wu, and Xiao[42–44] refined the apparatus and observed squeezed states produced in an optical parametric oscillator (OPO). The frequency doubled output of a ring Nd:YAG laser (0.53 μm) was used to pump a $MgO:LiNbO_3$ OPO. The Nd:YAG was frequency locked to an external cavity and had a linewidth of only 100 kHz. The resonator of the OPO was tuned to lock the OPO output to a radio frequency sideband of the 1.06 μm Nd:YAG fundamental. Balanced homodyne detection was performed by mixing the 1.06 μm Nd:YAG fundamental, a local oscillator, with the OPO output. Low-noise PIN photodiodes were used as detectors. An acousto-optical attenuator was used to reduce the Nd:YAG local oscillator power and thereby optically balance detection. Noise in the homodyne detector was suppressed by –4 dB under the shot noise limit (a 60% noise reduction).

There are many other examples of quadrature squeezing based on the parametric conversion[45–47] and other intracavity nonlinear interactions with both continuous and pulsed light sources,[45,48–51] nonlinear susceptibility in semiconductors,[52] and in optical fibers.[53–55] The best example of Breitenbach et al.[45] who not only demonstrate 5.5 dB squeezing with a monolithic OPO, but also perform exquisite statistical analysis of the resulting light. However, quadrature squeezed states are not easy to obtain or utilize. The many predicted applications have not followed. Most reports on applications of quadrature squeezed light have been theoretical. The main problem with quadrature squeezing based on nonlinear optical processes is that excess pump laser noise usu-

ally degrades the squeezed output[56] to the point where the squeezed light is only slightly better than the shot noise limit.

E. Detection of Squeezed States

There are three main techniques that may be employed to confirm quadrature squeezing. The first is to measure the photon count distribution with an ideal detector, that is, one with unit quantum efficiency. Squeezing would be indicated by a measured photon number distribution wherein the width of the distribution is not that expected based on the Poisson distribution. The theory predicts that the variance in the photon number should be less than that of the Poisson distribution for moderate squeezing parameters. This variance reduction occurs when both quadrature components are measured. Additionally, oscillations in the photon number distribution may be observed for high squeezing and low number counts. The latter measurements are not commonly used to detect quadrature squeezing, but have been used extensively to detect photon number-phase squeezed states discussed below. Correlation analysis, like the Hanbury Brown-Twiss experiment,[13-15] or temporal correlation analysis[8,16] may also be used to detect the quadrature squeezed states.

However, photon statistics and correlation measurements are based on fourth orders of the complex electromagnetic field amplitudes, whereas quadrature squeezing is a second-order effect.[31-33] A more straightforward method to measure quadrature squeezed light is therefore to use an interferometric technique wherein the noise statistics of each quadrature component can be measured. This is accomplished by mixing a local oscillator with variable optical phase with the squeezed light at a beamsplitter. The resulting light is detected with use of an optical balanced mixer and processed with power-law processing electronics, such as a spectrum analyzer. The frequency of the local oscillator may be different than that of the squeezed light. Measurements at the interference or beat frequency between the local oscillator and the squeezed light moves the measurement frequency out of the flicker noise and allows the use of an electronic spectrum analyzer. The relative phase of the two optical signals is varied with a piezoelectric mirror.

VI. PHOTON DETECTION STATISTICS

Many experimental measurements of the states of light have been based on noise spectral density measurements. Squeezed states of light may be detected by direct detection and reconstruction of the photon count distribution,[18,34] using balanced homodyne detection with a local oscillator,[6,36,37,57-59] or simply using a balanced mixer[60-62] similar to that used in the Hanbury Brown and Twiss experiments.

A. Balanced Detection

A balanced detector is illustrated in Figure 4. Here the optical radiation with a power Φ_0 is split into two nearly equal beams with powers Φ_1 and Φ_2. Differences in the optical powers or photodiode efficiencies are compensated by using a variable attenuator in one of the beams. Signals produced by the two photodiode detectors, i_1 and i_2, proportional to Φ_1 and Φ_2, respectively, are electronically processed. The sum, $\sum i = i_1 + i_2$, and difference, $\Delta i = i_1 - i_2$, current signals are amplified, and the noise power analyzed with a spectrum analyzer. The spectrum analyzer produces a signal that is the power spectrum of the noise in the sum and difference signals. In addition to allowing determination of the noise statistics, the balanced detector may reduce the influence of detector noise on the field/photon noise analysis. Analysis of the sum and difference currents

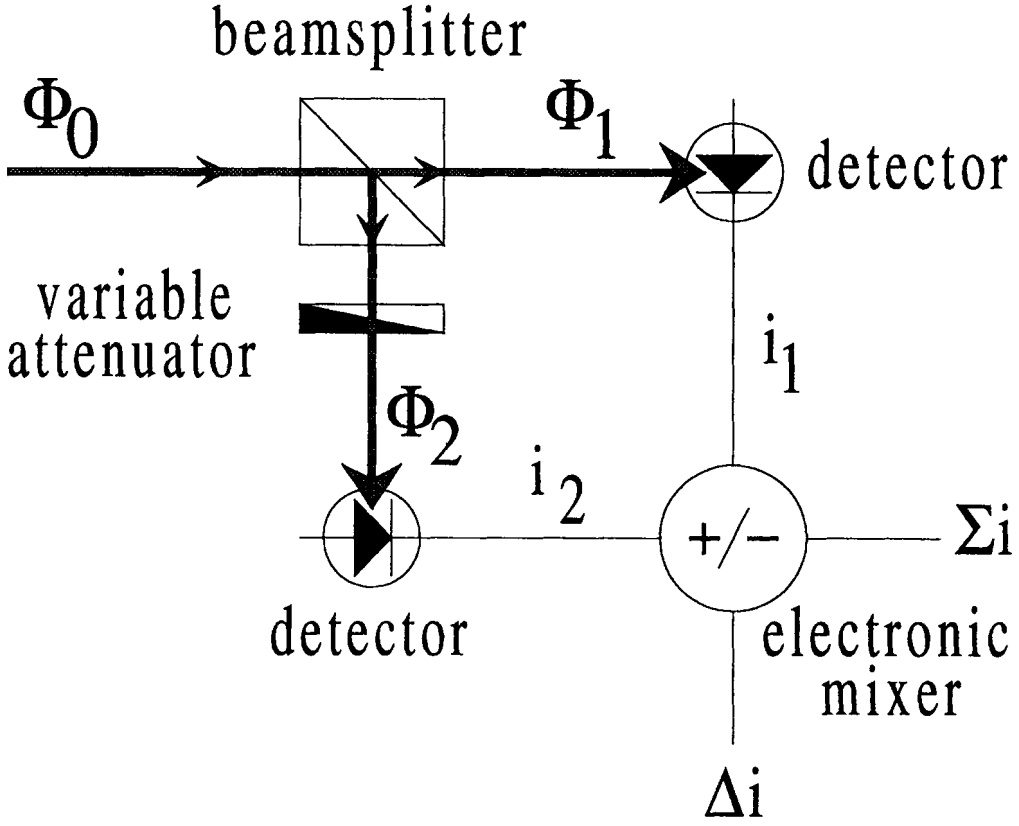

FIGURE 4. A balanced detector consisting of a beamsplitter and two detectors. The power in the two beams is balanced with the variable attenuator placed in one of the branches. Electrical current from the detectors is either added or subtracted, producing the sum, Σ, and difference, Δ, currents, respectively.

allows a convenient means to compare photon statistics to Poisson distributed coherent light.

Balancing the optical power, or rather the photodiode currents, by attenuation of the optical power in one branch can be troublesome. This is especially true if the incident radiation has random polarization. With polarized light, a polarizing beamsplitter in combination with a λ/2 plate placed in the Φ_0 beam can be used to balance the light between the two detectors.[37,57]

The statistics of the analysis will first be described using the photon count or charge accumulated in a charge-coupled device (CCD) detector, as it is easier to see twhat happens at the beamsplitter in this case. This treatment assumes that the intensity of light does not change in time. If the flux fluctuates on the time scale of the measurement, and if the photon detection events are not correlated, then the mean photon number at time t is the integral over the measurement time, T[8]

$$\langle n \rangle = \int_t^{t+T} \Phi_p(t')dt' \qquad (37)$$

Photon count means and variances are obtained through replicate measurements. Probability distributions may be obtained using multichannel analysis.

B. Beamsplitter Partitioning

The beamsplitter produces two beams, $\Phi_1 = X\Phi_0$, and $\Phi_2 = (1 - X)\Phi_0$, where $X \sim$

1/2. Splitting the beam into two components by the passive beamsplitter is a random process. The statistics of photon partitioning between the two beams are similar to Bernoulli trials, and are described by the binomial distribution[17]

$$P_n(n_1,n_2)=\frac{n!}{n!n!}X^{n_1}(1-X)^{n_2} \quad (38)$$

where n_1 and n_2 are the numbers of photon in beams Φ_1 and Φ_2 over the same period. For a loss-less beamsplitter, the total number of photons is conserved.

For an input beam with Poisson photon statistics, the photon statistics in resulting the split beams is the product of the Poisson input, $P(n,\langle n\rangle)$, and binomial partitioning, $P_n(n_1,n_2)$, PDFs, summed over all possible input beam n. For replicate samples of the input beam over a given time period, the average number of photons $\langle n\rangle$, with a measurement variance is $\sigma_n^2=\langle n\rangle$. Using $n=n_1+n_2$, the PDF for replicate measurements in either split beam can be found. For the Φ_1 beam

$$P(n_1)=\sum_{n=0}^{\infty}P(n,\langle n\rangle)P_n(n_1,n_2) \quad (39)$$

where the first PDF in the sum is the Poisson source and second is the binomial beamsplitter PDF. The summation can be evaluated, yielding

$$P(n_1)=\sum_{n=0}^{\infty}\frac{\langle n\rangle^n}{n!}e^{-\langle n\rangle}\frac{n!}{n_1!(n-n_1)!}X^{n_1}(1-X)^{n-n_1}$$

$$=\frac{(\langle n\rangle X)^{n_1}}{n_1!}e^{-\langle n\rangle X} \quad (40)$$

Clearly, binomial partitioning of photons between two beams results in Poisson photon statistics in each beam when the input beam is Poisson. The photon number mean and variance are given by the product of the input photon number with the efficiency of the partitioning to a particular beam. $\langle n_1\rangle=\langle n\rangle X$ for Φ_1 and $\langle n_2\rangle=\langle n\rangle(1-X)$ for Φ_2 with variances equal to the means in both cases. Recombining Φ_1 and Φ_2 beams is represented by the convolution of the individual PDF, $P(n_1)*P(n_2)$. Recombination results in the original input beam Poisson PDF, as the sum of two Poisson processes is a Poisson process. Similarly, the sum of photon counts produced by two perfect detector in the Φ_1 and Φ_2 beams would have mean, $\langle\sum n\rangle=\langle n\rangle$, and variance, $\sigma^2_{\sum n}=\langle n\rangle$.

An effect similar to the partitioning of photons at a beamsplitter occurs for any loss processes. Loss of photons, for example, with a less than unit quantum efficiency detector or loss due to optical absorption or scattering, is a random process equivalent to partitioning photons into a detectorless channel with a beamsplitter. In this case the process efficiency, or detector quantum efficiency, η, where $0\le\eta\le1$, takes the place of the beamsplitter ratio X.

C. Photons and Charge

The average charge produced in the detectors (producing a maximum of one charge carrier per photon detection event) over the sample period are $\langle q_1\rangle=\eta e\langle n\rangle X$ and $\langle q_2\rangle=\eta e\langle n\rangle(1-X)$, where e (C) is the electron charge, it is assumed that both detectors have the same quantum efficiency, η, and that the quantum efficiencies do not fluctuate. The photoelectric charges, q_1 and q_2, are measured directly when using an integrating detector (e.g., a CCD). (The later assumptions are generally not true. However, balancing can be used to account for efficiency differences. Fluctuations in quantum efficiencies is thought to be a fundamental flicker noise source in current generating detectors for example, Fang, P. et al., *J. Appl. Phys.*

1989, *65,* 1766]. This noise source may be detected and compensated for with spectral noise analysis. This $1/f$ and shot noise are probably not present in CCD devices [Van Vliet, C. M. *Solid-State Electron.* **1991,** *34,* 1].) The variance in charges measured with the detectors are $\sigma_q^2 = \eta e\langle q\rangle$.

Statistics of the detector difference signal is obtained from the PDFs for the individual charges. Defining the individual charge PDFs

$$P(q_1) = \frac{\langle q_1\rangle^{q_1}}{q_1!} e^{-\langle q_1\rangle}, \quad P(q_2) = \frac{\langle q_2\rangle q_2}{q_2!} e^{-\langle q_2\rangle} \tag{41}$$

where $\langle q\rangle$ are defined above, the PDF for the charge difference, $\Delta q = q_1 - q_2$, is

$$P(\Delta q) = \sum_{\Delta q = q_1 - q_2} P(q_1)P(q_2)$$

$$= e^{-\langle q_1\rangle - \langle q_2\rangle} \sum_{q_2=0}^{\infty} \frac{\langle q_1\rangle^{\Delta q}\left(\langle q_1\rangle + \langle q_2\rangle\right)q_2}{(\Delta q + q_2)!\,q_2!} e^{-\langle q_2\rangle} \tag{42}$$

The average and variance can be obtained by summing over Δq prior to the sum over q_2. The results are

$$\langle \Delta q\rangle = \sum_{\Delta q} \Delta q P(\Delta q) = \langle q_1\rangle - \langle q_2\rangle$$

$$\sigma_{\Delta q}^2 = \sum_{\Delta q} (\Delta q)^2 P(\Delta q) - \langle \Delta q\rangle^2 = \langle q_1\rangle + \langle q_2\rangle \tag{43}$$

Substituting the definitions for the $\langle q\rangle$, $\langle \Delta q\rangle = \eta e\langle n\rangle(2X - 1)$ and $\sigma_{\Delta q}^2 = \eta e^2\langle n\rangle$. For balanced signals, $X = 1/2$, and $\langle \Delta q\rangle = 0$. The differential charge variance is proportional to the photon number variance of the input beam regardless of whether the signals are balanced. The summed charge, $\Sigma q = q_1 + q_2$, is obtained from the convolution

$$P(\Sigma q) = \sum_{\Sigma q = q_1 + q_2} P(q_1)P(q_2)$$

$$= e^{-\langle q_1\rangle - \langle q_2\rangle} \frac{\left(\langle q_1\rangle + \langle q_2\rangle\right)^{\Sigma q}}{\Sigma q!} \tag{44}$$

The mean and variance of this Poisson distribution are

$$\langle \Sigma q\rangle = \sum_{\Sigma q} \Sigma q P(\Sigma q) = \langle q_1\rangle + \langle q_2\rangle$$

$$\sigma_{\Sigma q}^2 = \sum_{\Sigma q} (\Sigma q)^2 P(\Sigma q) - \langle \Sigma q\rangle^2 = \langle q_1\rangle + \langle q_2\rangle \tag{45}$$

which with the photon number-charge relationships yield $\langle \Sigma q\rangle = \eta e\langle n\rangle$ and $\sigma_{\Sigma q}^2 = \eta e^2\langle n\rangle$.

Important to note here is that the variance is produced from the optical photon number statistics, not the electron statistics. Presently, cooled CCD detectors with dark electron production rates on the order of a few electrons per hour are available so the statistics of the measurement charge are probably accurate without accounting for detector dark noise. The same result may be obtained assuming q_1 and q_2 come from a normal Gaussian distribution with equal means and variances, and applying of the usual propagation of errors procedure to determine the variance in the difference.

D. Photon Statistics of Ideal Squeezed Light

For the most ideal light, that is, zero photon number fluctuation, the beamsplitter produces two beams with statistics given by the binomial PDF. The PDF for photon number in the two split beams are

$$P_n(n_1) = \frac{n!}{n_1!(n-n_1)!} X^{n_1}(1-X)^{n-n_1}$$

$$P_n(n_2) = \frac{n!}{n_2!(n-n_2)!} X^{n-n_2}(1-X)^{n_2} \qquad (46)$$

These distributions have the means and variances: $\langle n_1\rangle = \langle n\rangle X$, $\langle n_2\rangle = \langle n\rangle(1-X)$, $\sigma_1^2 = \sigma_2^2 = \langle n\rangle X(1-X)$. The photon number variance is equal in both beams. This is because any random loss of photons from a given beam will result in random gain in the other beam. The variance is a maximum for $X = 1/2$, in which case $\sigma^2 = 1/4\langle n\rangle$, a factor or two less than that produced by splitting a Poisson-distributed coherent state input beam. On the other hand, the photon number fluctuations in the two detectors are correlated. A loss of photons from one split beam necessitates a gain in the other. The difference photon number between the two detectors is $\Delta n = n_1 - n_2$, which, on the average, is $\Delta n = \langle n\rangle(2X-1)$. The variance in photon difference is $\sigma_{\Delta n}^2 = 4\langle n\rangle X(1-X)$. With a perfect 50% beamsplitter, the photon number difference variance is $\sigma_{\Delta n}^2 = \langle n\rangle$, exactly that of a coherent input beam with Poisson photon statistics. This implies that the variance in the difference channel of the balanced mixer detection is a measure of the normal Poisson or shot-noise limit, independent of the statistics of the incident light.[34] The photon number measured by recombining the Φ_1 and Φ_2 beams, or, equivalently, by summing the photons counted by the two detectors, is obtained from the convolution of the two PDF. The photon number measured with the summed detector counts is $\sum n = \langle n\rangle$, whereas the variance is $\sigma_{\Sigma n}^2 = 0$. Thus, by comparing measurements of $\sum n$ to Δn, the photon statistics, in particular, the input beam variance, is compared to that of the coherent state.

The effect of finite detector quantum efficiency is similar to that of the beamsplitter. The process of charge production or photon energy loss is binomial, and the photon detection statistics are

$$P_n(k) = \frac{n!}{k!(n-k)!} \eta^k(1-\eta)^{n-k} \qquad (47a)$$

where k is the number of detected photon out of a total of n photons at a detector with quantum efficiency η. The photon number is readily converted to charge through multiplication by e, the electron charge. For the ideal photon source, the beamsplitter first changes the photon statistics in a reversible fashion, then the finite quantum efficiency further modifies these statistics irreversibly. The charge in each detector over the measurement period will be $\langle q_1\rangle = \eta e\langle n\rangle X$ and $\langle q_2\rangle = \eta e\langle n\rangle(1-X)$, and the individual variances are

$$\sigma_1^2 = e^2\langle n\rangle[\eta(1-\eta)X + \eta^2 X(1-X)] \text{ and}$$

$$\sigma_2^2 = e^2\langle n\rangle[\eta(1-\eta)(1-X) + \eta^2 X(1-X)] \qquad (47b)$$

These are obtained using $\sigma_k^2 = \langle k^2\rangle - \langle k\rangle^2$ and the distribution found from the convolution of the beamsplitter partition noise PDF with the finite quantum efficiency PDF, $P_n(k) = P_n(n')*P_{n'}(k)$. The first terms of these variances, proportional to $\eta(1-\eta)$, are due to finite detector quantum efficiency photon loss, whereas the second terms, proportional to $X(1-X)$, are the partitioning noise due to the beamsplitter. The average summed charge is $\langle \sum q\rangle = \eta e\langle n\rangle$, whereas the variance is $\sigma_{\Sigma q}^2 = \eta(1-\eta)e^2\langle n\rangle$. The average difference charge is $\langle \Delta q\rangle = \eta e\langle n\rangle(2X-1)$ with a variance of $\sigma_{\Delta q}^2 = e^2\langle n\rangle[\eta(1-\eta) + 4\eta^2 X(1-X)]$. With a balanced beamsplitter, the average difference charge is zero, whereas the variance is $\eta e^2\langle n\rangle$. Again, this variance is that which would be obtained from a coherent beam with Poisson photon number statistics and the variance of the difference signal can be used to gauge the variance in the sum signal to the shot-noise limit.

E. Interpreting Photons Statistics from Balanced Mixer Detection

Practical squeezed light is less than ideal. The light may be thought of as being part

coherent and part squeezed. The photon statistics will be between the two limiting cases, depending on the degree of squeezing. In general, photon statistics of the Φ_0 input beam can be gauged relative to that of a coherent beam using the balanced detector. The variances in the sum and difference counts or currents are $\sigma^2_{\Sigma q} = e^2(\sigma_1^2 + \sigma_2^2 + 2\langle\Delta n^2\rangle)$ and $\sigma^2_{\Sigma q} = e^2(\sigma_1^2 + \sigma_2^2 - 2\langle\Delta n^2\rangle)$. The σ_1^2 and σ_2^2 are the variances in each channel. $\langle\Delta n^2\rangle$ is the expectation of the correlated photon detection events, defined through the cross-correlation, $R_{1,2} = \langle n_1 n_2\rangle$, or $R_{1,2} = \langle\langle\langle n_1\rangle - \Delta n)(\langle n_2\rangle - \Delta n)\rangle$ for Δn correlated fluctuations from the means. Because $\sigma^2_{1,2} = R_{1,2} - \langle n_1\rangle\langle n_2\rangle$, $\langle\Delta n^2\rangle = \sigma^2_{1,2}$ is the covariance defined in the usual fashion.[17] It is also related to the second-order coherence function. The second-order coherence function is the relative correlation $g^{(2)}(x_1,x_2) = R_{1,2}/\langle n_1\rangle\langle n_2\rangle$ by $g^{(2)}(x_1,x_2) = 1 + \langle\Delta n^2\rangle/\langle n_1\rangle\langle n_2\rangle$. If photon numbers are obtained with a unit quantum efficiency detector, the second-order coherence function related to the sum and difference charge variances by $g^{(2)}(x_1,x_2) = 1 + (\sigma^2_{\Sigma q} - \sigma^2_{\Delta q})/4\langle q_1\rangle\langle q_2\rangle$.

Another useful parameter for characterizing photon statistics is the Fano factor, F.[9] The Fano factor is defined as the ratio of the expectations of photon number variance to photon number $F = \sigma_n^2/\langle n\rangle$. The Fano factor is 1 for Poisson distributed photon distributions produced by coherent light. Light with Fano factors less than one is said to be sub-Poisson because the variance is less than that of the Poisson distribution. Sub-Poisson light indicates squeezed states or anti-bunching. Super-Poisson light is indicated by a Fano factor greater than one. The bunched photons produced by thermal sources result in super-Poisson light because the photon number variance $\sigma_n^2 = \langle n\rangle + \langle n^2\rangle$, is greater than the expectation $\langle n\rangle$ for large photon numbers. Inasmuch as the variance in photon number is the Poisson or shot noise limit, the Fano factor is simply the ratio of sum and difference variances, $F = \sigma^2_{\Sigma q}/\sigma^2_{\Delta q}$, measured with the well-balanced (i.e., $X = 0.5$) detector. The Fano factor of the light can be found from the measurements using the relationship $\eta(F - 1) = F_\eta - 1$, where F is the Fano factor of the light and F_η is that for the detected light. Finite detector quantum efficiency causes the Fano factor to be closer to unity, that is, more Poisson, than that of the light source, independent of whether the light is sub-Poisson or super-Poisson. For a series of loss processes with transfer efficiencies α_i, the overall efficiency is $\eta = \Pi\eta_i$. Efficiency loss occurs at all optical interfaces and with absorbing or scattering samples.

F. Detector Current

Solid-state or vacuum photodiodes and photomultiplier tube detectors produce current signals. Photon number and photon rate distributions are related by $\langle n\rangle = \Phi_p t$, where Φ_p (s^{-1}) is the photon flux (in quanta per second). So all the photon number PDF can be cast in terms of the rates. Photon rates are converted to currents by a detector. Detector currents are proportional to the rates of photon annihilation and subsequent electron or electron-hole pair production in the detector. Under the assumption that no shot noise is generated at the photocathode of the vacuum devices, or in the junction of the solid-state semiconductor photodiode, and that there is no flicker noise, the noise measured using current detectors to measure the optical radiation is proportional to fluctuations in photon rates. These assumptions may not be valid, particularly at high optical power. The validity is highly dependent on the particular type and structure of the device. The texts by Smullin and Haus[63] and van der Ziel[64] contain information regarding fundamental noise sources in electron and semiconductor devices. On the other hand, basic assumptions regarding the photocurrent-induced noise processes have not been tested in most devices. This is due to the fact that the optical

sources used to measure the noise in these devices have been thermal or coherent sources.

Detector currents are combined to produce the sum and difference currents $\sum i$ and Δi. The currents are usually processed with a spectrum analyzer. The spectrum analyzer measures the frequency-dependent signal power. The spectral density, $S(\omega)$, of a signal is the Fourier transform of the autocorrelation function. For example, defining the autocorrelation for the difference current,

$$R_\Delta(\tau)\langle\Delta i(t+\tau)\Delta i(t)\rangle = \lim_{T\to\infty}\frac{1}{T}\int_0^T \Delta i(t+\tau)\Delta i(t)\,dt \quad (48)$$

the spectral density is

$$S_\Delta(\omega) = \mathcal{F}\{R_\Delta(\tau)\} \quad (49)$$

where $\mathcal{F}\{\ \}$ is the Fourier transform

$$\mathcal{F}\{R_\Delta(\tau)\} = \int_{-\infty}^{\infty} R_\Delta(\tau)e^{i\omega\tau}\,d\tau \quad (50)$$

Using the autocorrelation property of Fourier transforms[65]

$$S_\Delta(\omega) = \mathcal{F}\{\Delta i(t)\} * \mathcal{F}\{\Delta i(t)\} = |\Delta I(\omega)|^2 \quad (51)$$

where $\Delta I(\omega)$ is the Fourier transform of $\Delta i(t)$. On a microscopic scale, current is produced by either electron-hole production in the solid state detector or photoelectron production at the photocathode of a vacuum photodetector. The individual charge production event when a single photon is annihilated is an instantaneous delta function process, that is, the charge either exists or it does not. Subsequently, the intrinsic spectrum of the photon detection process is "white" because the Fourier transform of a delta function is a constant. The magnitude of the spectral density is proportional to the rate of these delta function events (i.e., the current). The shot noise power, or current variance, is proportional to the bandwidth of the measurement. With a factor of 2 correction for the Nyquist sampling interval, the shot noise variance $\sigma_i^2 = 2e\langle I\rangle\delta f$, where δf (Hz) is the frequency interval. This well-known formula is valid only if the rate is a Poisson process. Flicker noise, due both to the optical source and the detector and related circuitry, will persist at low frequencies.

As in the case of photon number or charge number detection, the statistics of the sum and difference currents will vary depending on the state of light entering the balanced detector. For continuous sources, the DC (zero-frequency) component of the spectral density contains information regarding the magnitude of the signal, whereas higher frequencies reflect the photon statistics of the source. In practical analysis, only the high frequency components of the spectral density are used to deduce photon statistics because of flicker noise in the source and detectors. For frequencies well away from the flicker noise roll off, variances in the sum and difference currents are $\sigma_{\Sigma i}^2 = S_{\Sigma i}(\omega)$ and $\sigma_{\Delta i}^2 = S_{\Delta i}(\omega)$. These variances may be used to deduce the second-order correlation function through $g^{(2)}(x_1, x_2) = 1 + (\sigma_{\Sigma i}^2 - \sigma_{\Delta i}^2)/4\langle i_1\rangle\langle i_2\rangle$, and the Fano factor through $F = \sigma_{\Sigma i}^2/\sigma_{\Delta i}^2$.

G. Homodyne Detection

Balanced detectors are useful for determining the photon statistics for a single beam. In quadrature squeezed light, not only are the photon statistics different than that of coherent or thermal radiation, but also the phase of coherent radiation is altered as well. Phase-sensitive detection is used to measure differences in phase certainty between the squeezed and classic states. This is accomplished by applying the homodyne detection. The difference between homodyne and the more common heterodyne detection techniques are discussed by Yariv.[6,57]

Heterodyne detection uses optical mixing of a local oscillator to the signal to be analyzed.[57] The optical frequency of the local oscillator is slightly different than that of the signal. The squared sum of two similar trigonometric functions can be represented as trigonometric functions of the sum and difference frequency components. The sum and difference frequencies occur at side bands from the carrier. The upper side band is well above frequencies able to measured electronically. However, the lower side band (LSB) contains the difference frequency components, which subsequently are analyzed electronically. Optical mixing is performed by superimposing two beams of light onto a single 'square-law' detector. The detector produces an electronic LSB signal (the upper side band is not at frequencies able to be detected with electronic circuits) at a frequency equal to the difference in optical frequencies between the two beams. An electronic band pass filter or spectrum analyzer is used to measure the signal at the optical beat frequency. Heterodyne detection can increase measurement sensitivity of the signal beam by orders of magnitude for detectors possessing dark current and Johnson noise. When shot noise due to the local oscillator prevail over all other noise sources, heterodyne detection yields quantum or shot noise limited detection of low-level signals. This limit corresponds the detection of one photon in a time equal to the inverse bandwidth of the measurement.

Homodyne detection differs from heterodyne in that local oscillator and signal beams are mixed at a beamsplitter, and two detectors are used to monitor the in-phase and out-of-phase components of the resulting superimposed fields in a balanced mixer configuration.[6,43] This process is illustrated in Figure 5. Difference frequency generation may be used in the same fashion as in heterodyne detection, that is, summation of the two electric fields followed by detection with a square law detector. The phase of the local oscillator is changed using a variable optical delay. Yariv[6] gives the resulting current signal as a function of the relative phase shift of the local oscillator, ϕ_{LO}.

$$\Delta i(\phi_{LO}) = i_0\left[\alpha_1(t)\sin\left(\phi_{LO}+\frac{\pi}{4}\right) + \alpha_2(t)\cos\left(\phi_{LO}+\frac{\pi}{4}\right)\right] \quad (52)$$

where only the difference current is monitored. The amplitude of the quadrature components can be analyzed by changing the phase of the local oscillator. However, the $\alpha(t)$ will time average to zero. In order to analyze the noise statistics, the difference current is not directly measured but rather analyzed with a spectrum analyzer. The spectrum analyzer processes the power in the individual frequency components. The power, in turn, is proportional to the squared detector difference current. Analyzing the difference current as the square results in a direct measurement of the degree of squeezing through

$$\left\langle\left(\frac{\Delta i(\phi_{LO})}{i_0}\right)^2\right\rangle = \frac{1}{4}\left[e^{2r}\sin\left(\phi_{LO}+\frac{\pi}{4}\right) + e^{-2r}\cos\left(\phi_{LO}+\frac{\pi}{4}\right)\right] \quad (53)$$

The noise amplitude as a function of quadrature phase may also be analyzed when the local oscillator is phase locked to the signal. In this case the relative phase of the two beams is varied using a variable phase plate in the local oscillator. The phase-sensitive analysis is particularly revealing of the noise statistics of quadrature squeezed light.

Wu et al.[43] derive a formula relating the power spectrum of the quadrature squeezed light within an OPO to the homodyne measurements. Their analysis was extended by Breitenbach et al.[45] to include analysis of the of the photon statistics and probability density function of both quadratures. In these

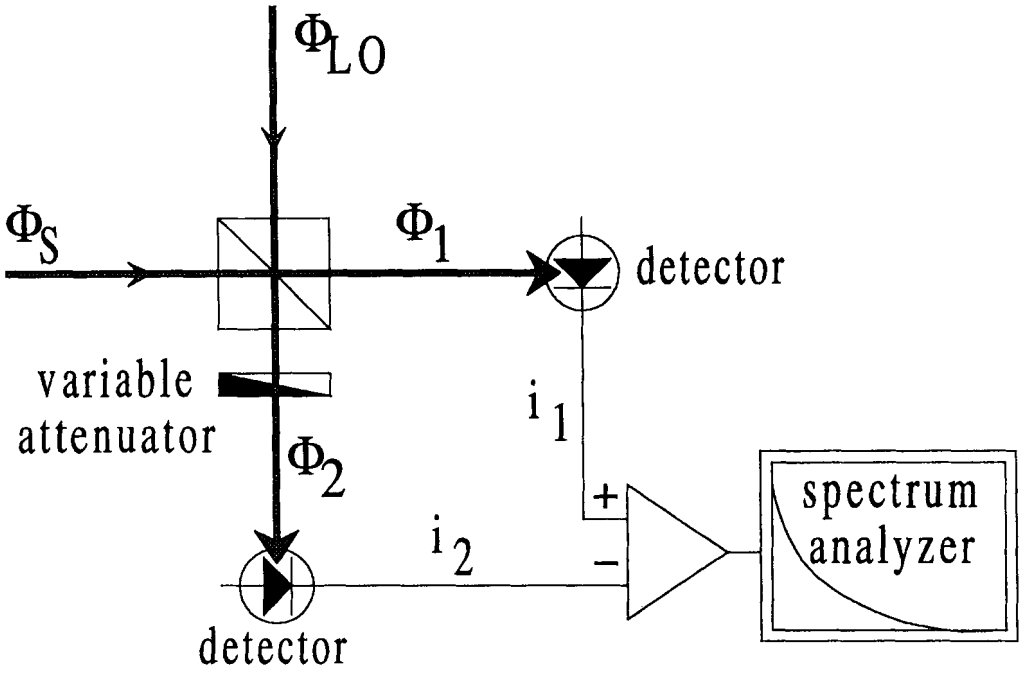

FIGURE 5. Homodyne detection. Signal, Φ_S, and local oscillator, Φ_{LO}, beams are combined at the beamsplitter. Two detectors are used to monitor the power in the two branches of the combined beams. The difference detector current is produced and subsequently processed with a spectrum analyzer.

examples, both the detector current difference and sum statistics are determined. The photon statistics of the local oscillator, a real laser, often has noise in excess of a pure coherent state. Subsequently, it is difficult to detect quadrature squeezing because the lower classic noise limit is not known *a priori*. This problem can be overcome by measuring noise statistics at photodetector current summing junction in addition to the difference junction.[43] As shown above, the variance at the current summing junction will indicate the shot noise limit. In addition, The noise spectrum of the LSB of the two mixed beams may be analyzed, revealing the noise power spectrum. This in turn may be used to gauge the excess flicker type noise as well as the frequency range over which squeezing occurs. The latter may be influenced by the response time of the nonlinear system used to generate the squeezed state.

A large part of the literature on quadrature squeezed light refers to an effect called "squeezed vacuum".[36,41,53,66–67] A squeezed vacuum is simply the reduction in noise power to below the shot noise limit obtained when a quadrature squeezed state is mixed with the local oscillator over that of the local oscillator alone. In effect, noise in the local oscillator quadrature component corresponding to the squeezed input signal is reduced below the shot noise limit when the quadrature squeezed signal is present. The noise limit due to shot noise is measured by blocking the quadrature squeezed signal light. Further, by analyzing the difference in detector current, excess noise in the local oscillator is reduced.

Squeezed vacuum is confirmed from the power spectrum obtained using the balanced optical homodyne detector. For a given laser power used to pump the OPO or P (W), the power spectra of the squeezed, $S_-(\omega)$, and anti-squeezed, $S_+(\omega)$ (Hz^{-2}), components of the light are[45]

$$S_{\pm}(\omega) = \pm \frac{4\sqrt{P/P_{th}}}{(\omega/\Gamma)^2 + \left(1 + \sqrt{P/P_{th}}\right)^2} \qquad (54)$$

where P_{th} (W) is the threshold power for OPO operation and Γ (Hz) is the OPO cavity bandwidth. The power spectra measured from the difference detector current mixing point is

$$R_{\pm}(\omega) = R_0[1+\rho\eta S_{\pm}(\omega)] \quad (55)$$

where R_0 is the spectral density for the vacuum input, obtained from the summed currents, ρ is the OPO resonator escape efficiency, and η is detector efficiency. When the relative phase of the local oscillator is set to analyze the squeezed quadrature, the spectral density is less than the vacuum or shot noise limit, R_0, because $S_{\pm}(\omega)$ is negative for squeezed component. On the other hand, when the relative phase is set to analyze the anti-squeezed component, the noise power is super-Poisson. The frequency dependence, ω (rad s^{-1}), of the squeezed vacuum is also important. Greater squeezing bandwidths allow for a wider range of applications. In general, the low-frequency end of the squeezed vacuum noise power spectrum is dominated by flicker-type excess noise in the local oscillator, whereas the high-frequency end is limited by the response time of the device used to obtain the squeezed light. The high radio frequency cut-off bandwidth of quadrature squeezed states produced using nonlinear optical materials placed in cavities to enhance the interaction is limited by the cavity lifetime. Thus, although high Q cavities have enhanced quadrature squeezing, their use produce lower bandwidths over which squeezing occurs.

Figure 6 illustrates the data obtained by Breitenbach et al.[45] using the homodyne-balanced mixer. Although these data do illustrate squeezing at a certain phase of the local oscillator, they do not show the relative variance in the quadrature components. The quadratures components, $\hat{x} = (\hat{a} + \hat{a}^{\dagger})$ and $\hat{p} = i(\hat{a}^{\dagger} - \hat{a})$, are the position and momentum operator equivalents derived from the field operators, respectively. The electric field variance is then $[\Delta\hat{E}(\theta)]^2 = (\Delta\hat{x})^2 \cos^2\theta +$

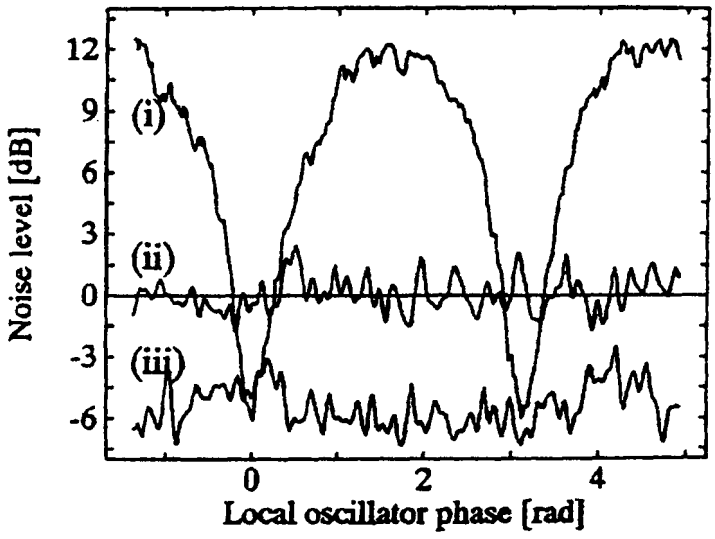

FIGURE 6. Data obtained using a homodyne detection apparatus for squeezed light produced using an optical parametric amplifier. Trace (i) is that obtained when the local oscillator phase is scanned. Trace (ii) is the shot noise limit obtained without phase scanning, while trace (iii) is that obtained by fixing the local oscillator phase for minimum noise. (Adapted from Breitenbach et al.[45] Figure 4.)

$(\Delta\hat{p})^2 \sin^2 \theta$. When plotted in polar coordinates, the local oscillator phase-dependent field standard deviation resembles a lemniscate with quadrature squeezing. The local oscillator phase-dependent variance data are replotted in Figure 7. Part **a** shows the variance data as black dots. The circle in the center is that of the shot noise limit and the smooth lemniscate curve is the model prediction. The principle axes, $a = \Delta\hat{x}$ and $b = \Delta\hat{p}$, correspond to the maximum squeezed and noise-enhanced quadrature components. The data illustrated in Figure 7 part **b** have been replotted and indicate the uncertainty region. It is a plot of the $[r(\theta) \cos \theta, r(\theta) \sin \theta]$ data pairs transformed to $[1/r(\theta)][a^2 \cos \theta, b^2 r(\theta) \sin \theta]$ coordinates.

Figure 7 part **b** data are contours of the full Wigner function for a quadrature squeezed state. Breitenbach et al.[45] also used a local oscillator that was ~2 MHz different than that of the OPO output. The relative

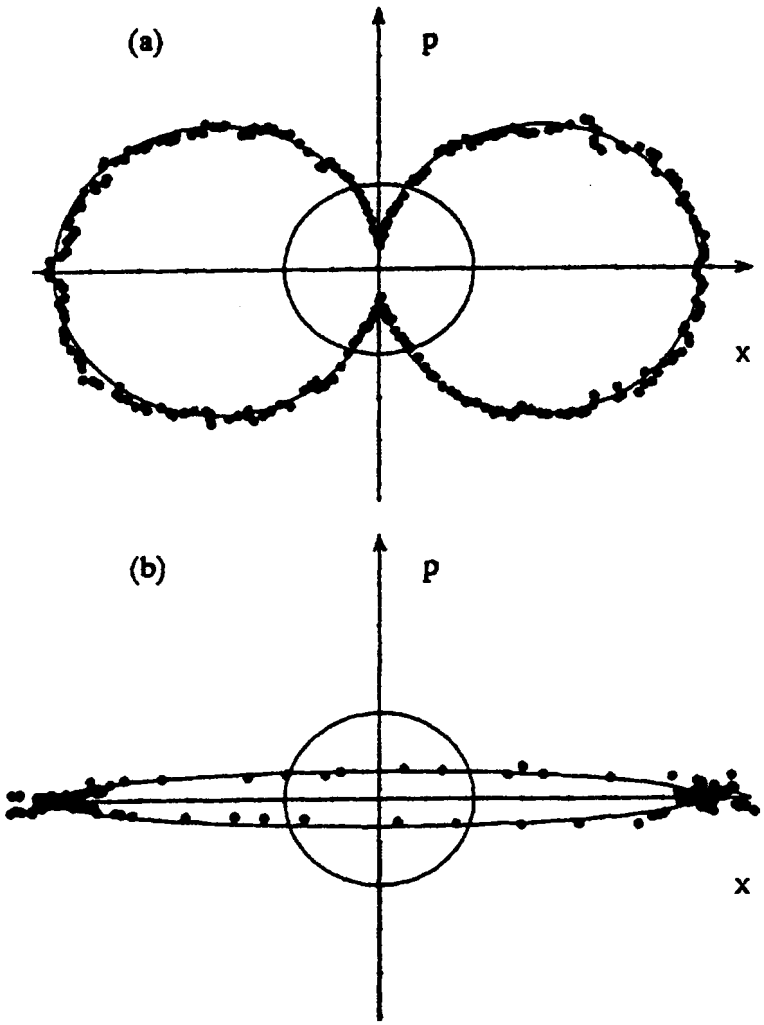

FIGURE 7. Two views of field standard deviation data obtained by changing the phase of the local oscillator in a homodyne detector. Part (a) is a polar plot of the homodyne signal standard deviation. The standard deviation is plotted as a function of phase angle. Part (b) is the same data transformed to illustrate the squeezing ellipse. The width of the ellipse is proportional to the standard deviation in this case. (Adapted from Breitenbach et al.[45] Figure 5.)

phase of the local oscillator thus changed continuously in time. The current was measured directly and noise amplitude was analyzed as a function of the relative phase. The data are shown in Figure 8. Noise amplitudes were found to fit a Gaussian distribution and the local oscillator phase-dependent variances were assessed (Figure 8 part **b**). This detailed analysis allowed the construction of plots revealing the amplitude fluctuations in the individual quadrature components. The analysis also allowed construction of the Wigner distribution, $W_{sq}(x,p)$

$$W_{sq} = \frac{1}{2\pi}\exp\left[-\frac{1}{2}\left(\left[1+\rho S_{-}(\omega)\right]x^2 + \left[1+\rho S_{+}(\omega)\right]p^2\right)\right] \qquad (56)$$

In turn, the Wigner function is related to the density matrix through a Fourier trans-

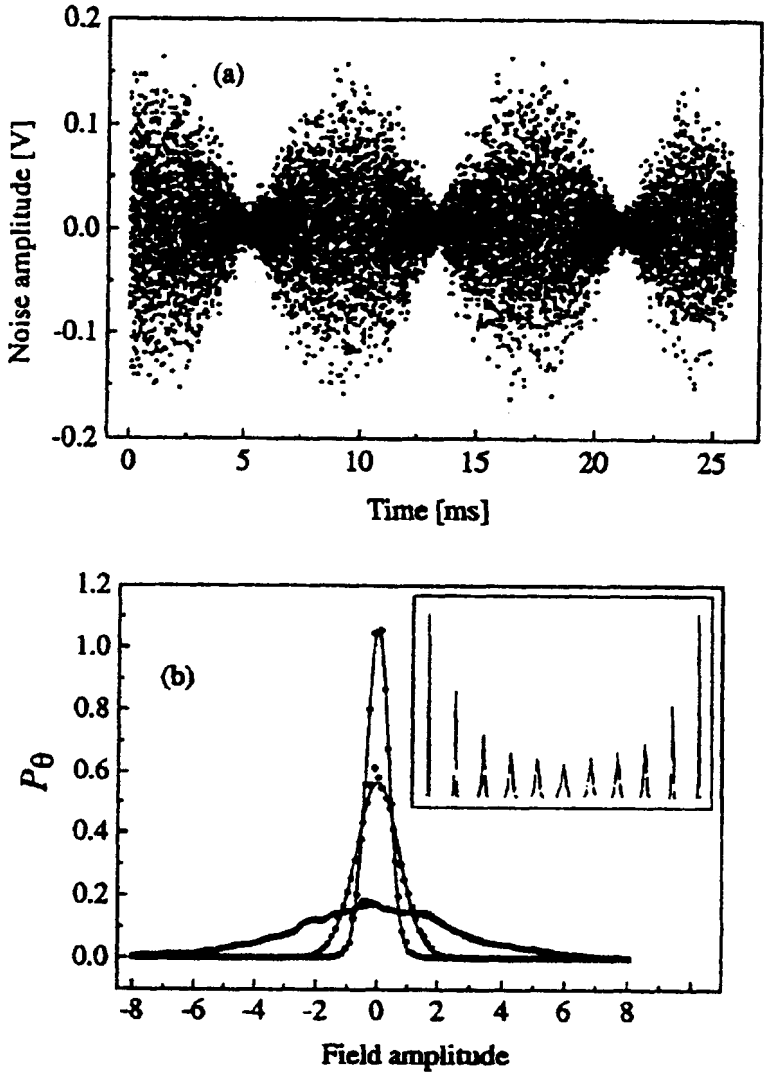

FIGURE 8. Data obtained by mixing a de-tuned local oscillator with the signal beam in the homodyne detector. Part (a) shows the signal evolution as the relative phase of the signal and local oscillator change. Part (b) shows probability density functions obtained by analysis of data in part (a) as a function of relative phase shift. (Adapted from Breitenbach et al.[45] Figure 6.)

form. Breitenbach et al. were able to confirm the degree of squeezing and anti-squeezing in the two quadrature components by fitting the phase angle-dependent noise amplitude variance data to the Wigner function by the data. This was done using a constrained Radon transform.[68,69] The resulting experimental Wigner function corresponded to 5.5 dB of squeezing and 11 dB of anti-squeezing, in agreement with simpler data analysis shown in Figure 6. The shape of the Wigner function had only been implied in work leading up the this report.

VII. NUMBER-PHASE SQUEEZED STATES

A. Basic Properties

In quadrature squeezed states the field amplitude variance of one of the two quadrature components of the electric field is reduced at the expense of the other. In amplitude or photon number squeezed states of light, the variance in photon number is reduced at the expense of the phase variance. Yamamoto et al., introduced the amplitude squeezed state in 1986[12,34] and have illustrated several means for sub-Poisson light generation since the initial report.

Quadrature component squeezed light results in an ultimate photon variance of $\sigma_n^2 \approx \langle n \rangle^{2/3}$.[29] A simple reason for this limitation is that squeezing the field amplitude fluctuation in one quadrature component requires an increase in the fluctuation of the other component in order to satisfy the product uncertainty principle. Too much squeezing increases the photon number fluctuation through the increase in the anti-squeezed quadrature fluctuation. Because photon number is proportional to the squared electric field, large field fluctuations of the anti-squeezed component can increase the photon number fluctuation.

The uncertainty principle may be satisfied with minimum-uncertainty photon-number phase states.[34,70] In this representation, minimum-uncertainty states are those that satisfy the relationship, $\langle (\Delta n)^2 \rangle \langle (\Delta \phi)^2 \rangle = 1/4$. The photon number variance is $\langle (\Delta n)^2 \rangle = \langle n \rangle$, so the minimum-uncertainty phase variance is $\sigma_\phi^2 = \langle (\Delta \phi)^2 \rangle = 1/4\langle n \rangle$. For coherent light, the photon number variance increases with the mean number of photons detected, whereas the phase variance is inversely proportional to the number of photons. The uncertainty principle is still valid in the field amplitude representation. However, the shape of the field amplitude space uncertainty profile is not elliptic, as in the case of the quadrature squeezed states, but rather is crescent shaped. This is illustrated in Figure 9. The photon number is proportional to the square of the two quadrature field amplitudes. Thus, the photon number is the square of the distance from any point on the graph to the origin. The variation of this distance is reduced with photon number squeezing. Similarly, the phase of the field is the angle a vector from the origin to any point makes with the horizontal quadrature axis. Part **A** of Figure 9 shows the result of partial minimum uncertainty photon number squeezing. The phase variance increases while the variation of distance to the origin decreases due to photon number squeezing. Part **B** shows the quadrature plot optimally squeezed photon number. The phase angle variance is extreme in this case. Minimum uncertainty phase squeezed states of light may also exist. The quadrature plot of this state would be similar to that shown in part **C** of Figure 1. In this case, phase angle variance is decreased at the cost of the average field.

B. The Nonlinear Interferometer

A relatively simple method for anti-bunching of photon distribution uses nonlinear optical transitions to selectively remove the photon pairs that are bunched. Although intuitive, there are some interesting consequences regarding the use of coherent and

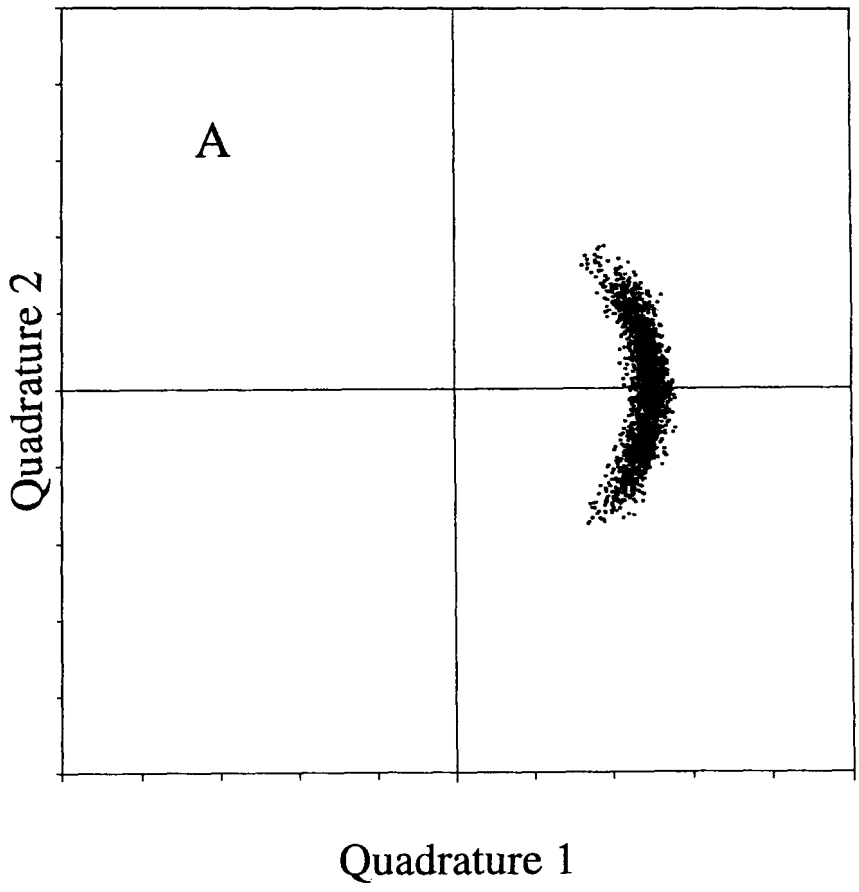

A

FIGURE 9. Probability density plots of a photon number-phase squeezed state. Part (A) illustrates uncertainty in the two fields produced with partial photon number squeezing. Part (B) corresponds to states where the phase variance is maximized while minimization of photon number fluctuations occur.

chaotic thermal light sources. Kitagawa and Yamamoto[34] analyze photon number squeezed states produced by mixing two beams, one from a coherent source and another the vacuum fluctuation or probe beam, within a nonlinear Mach-Zehnder interferometer. The scheme for production of photon number squeezed states is illustrated in Figure 10. Light (or vacuum fluctuations) from the two input ports are mixed at the first beamsplitter. The light is self-phase modulated by passing through a nonlinear optical Kerr effect medium placed in one of the interferometer paths. The phase of this path is changed by the intensity-dependent refractive index of the Kerr effect medium. For squeezed photon number, a higher intensity beam causes a phase shift that reduces the intensity in the output beam past the exit beamsplitter. The reflectivity of the beamsplitter is kept as high as possible to avoid contamination of the photon number squeezed state with noise from the vacuum or reference beam. Essentially, the scheme acts as an all-optical limiter wherein the phase of one beam is instantaneously changed to compensate for increased or decreased intensity. Thus, it may be simpler to obtain photon-number squeezed light using this or similar schemes than to obtain quadrature squeezed states. Moreover, unlike schemes based on the use of an optical cavity to increase the field to the point where nonlinear interactions take place, the bandwidth

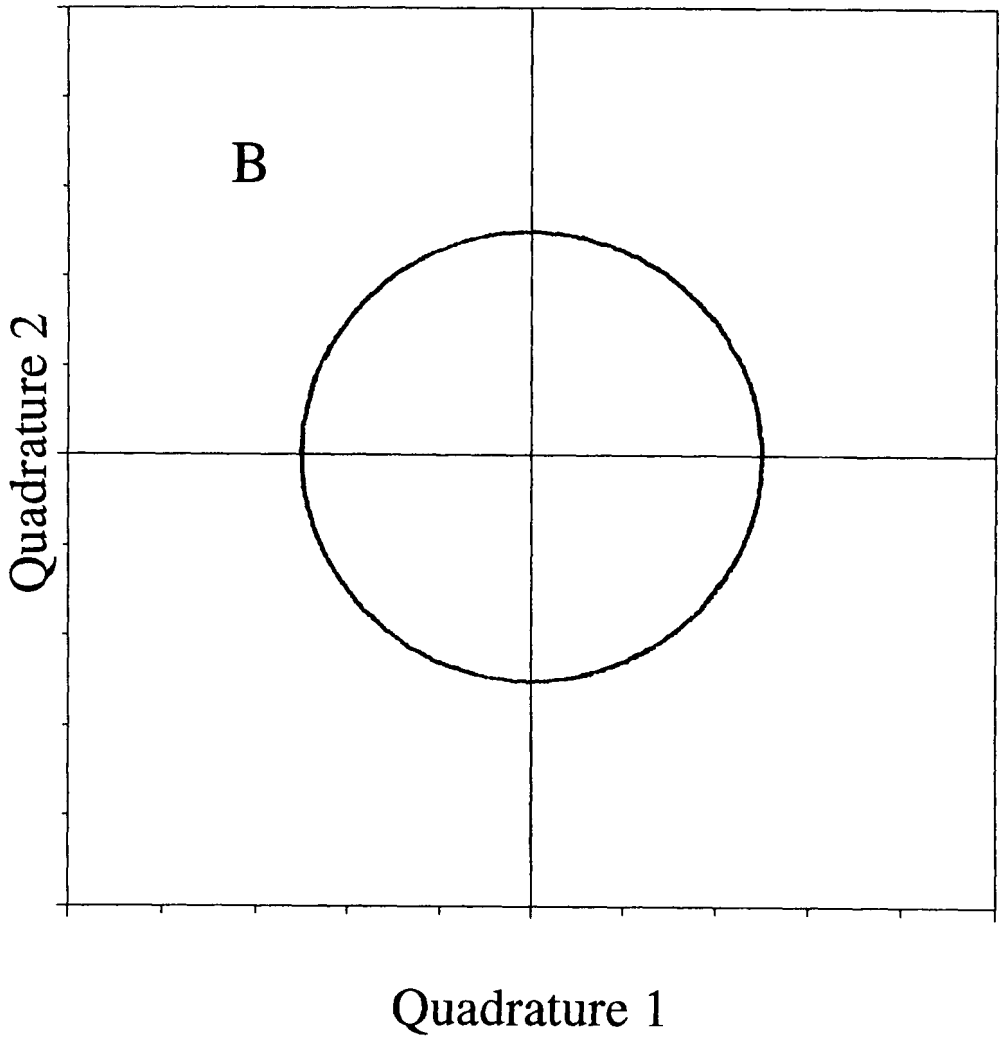

FIGURE 9B

of the photon number squeezing could be high, limited by the response time of the nonlinear Kerr effect media, not by cavity lifetime.

The photon states produced by the Kerr-effect interferometer can be described in terms of the parameters of the device. Given an annihilation operator for the photon number squeezed light $\hat{c}$ that follows the boson commutation relationship $[\hat{c},\hat{c}^\dagger] = 1$ and the photon number relationship $\hat{c}^\dagger\hat{c} = n$, the photon number squeezed states are related to the coherent input state by

$$\hat{c} = e^{i\gamma\hat{a}^\dagger\hat{a}}\hat{a} + \xi \qquad (57)$$

Here, γ is a parameter related to the efficiency of the nonlinear phase shift in the Kerr medium, and the ξ parameter is related to the coupling efficiency of the phase-shifted and unperturbed beams at the beamsplitter. γ can be arbitrarily increased by increasing the nonlinear Kerr medium interaction length. On the other hand, ξ is fixed by the beamsplitter or chosen for optimum squeezing in numerical modeling. The magnitude of γ will affect the phase shift for a given field. The interplay between γ and ξ will affect photon number fluctuations at the output ports. For a given ξ and average field amplitude, γ may be chosen to minimize

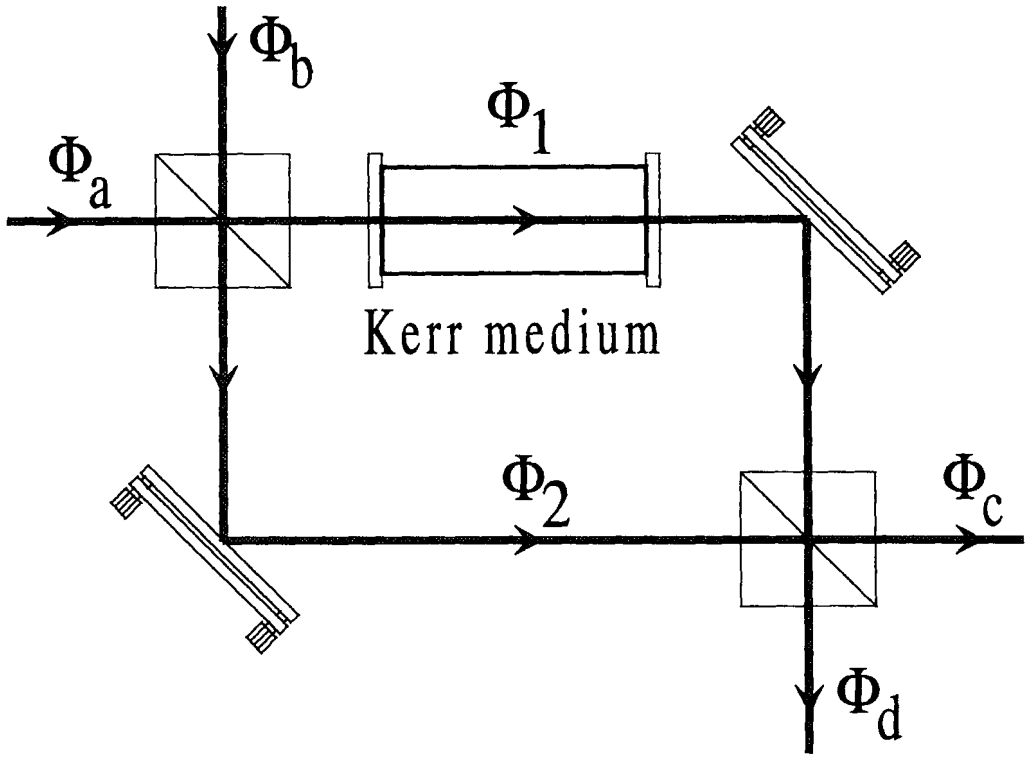

FIGURE 10. A nonlinear Mach-Zehnder interferometer used in the analysis of photon number squeezed states. One branch of the interferometer contains a nonlinear optical Kerr effect medium.

photon number fluctuations at the output port with electric field operator, $\hat{c}$. The photon number probability density function obtained from the density matrix is shown to be

$$P(n;\xi,\gamma) = e^{-(|\alpha|^2+|\xi|^2)}\frac{1}{n!}\left|\sum_{k=0}^{n}\sum_{m=0}^{\infty}\frac{n!\xi^k(-\xi^*)^m\alpha^{n-k+m}}{k!m!(n-k)!}e^{(i/2)\gamma(n-k+m)(n-k+m-1)}\right|^2 \tag{58}$$

This PDF is similar to the Poisson distribution but may have variances less than those of coherent light. It produces photon distributions that are more symmetrical than those of the quadrature squeezed light. The minimum variance produced by photon number squeezed states is found to be $\sigma_n^2 = \langle n\rangle^{1/3}$. However, the number variance can be reduced even further by cascading nonlinear optical Kerr effect interferometers at the cost of reduced average photon number.

C. Optical Feedback

The nonlinear Mach-Zehnder interferometer scheme described above is just one of several possible schemes that use rapid feedback to control the state of the field.[9] Yamamoto et al.[12] describe two other means for producing photon number or amplitude squeezed states. The first is based on a nondestructive, quantum demolition detection scheme. This scheme was only a theoretical construct used to develop the theory for the photon number squeezing through feedback. Nondemolition detection of a signal laser field was modeled using a probe laser to

detect the nonlinear phase shift produced in the nonlinear Kerr medium by the signal beam. This scheme is illustrated in Figure 11. The signal beam enters the interferometer through the upper input port of the interferometer, passing through a dichroic mirror. The mirror is coated to reflect the probe laser while transmitting the signal beam. The signal beam interacts with the optical Kerr medium and exits the interferometer through a second dichroic mirror. The probe beam enters the interferometer through the lower input port. This beam is split into two separate beams: one passing through the nonlinear Kerr medium, the second passing to the second beamsplitter. The probe laser wavelength is such that the reflectivity at the dichroic mirrors is high and the light does not affect the refractive index of the nonlinear medium. The probe beam is recombined at a second beamsplitter. The light from one of the output ports of this beamsplitter is detected. The amplitude of the light exiting this port is influenced by the phase shift incurred passing through the nonlinear Kerr medium, which in turn, is proportional to the signal laser field. The current from the detector is fed back to the signal laser. The lower the signal laser beam field, the higher the current to the laser. The hybrid nondemolition optical-electronic detection controls the field of the signal beam while not annihilating the signal photons. The bandwidth of the photon number squeezing should be very high for nonlinear Kerr effect media with fast response times. However, it will also be limited by the response time of the electronic detection and amplification circuits. This scheme will work for high quantum efficiency laser, such as diode lasers, wherein the number of photons produced is nearly equal to the number of electrons that pass through the band gap region. Moreover, noise in the probe beam will be reflected in the modulated signal beam. A high-power probe laser with minimum flicker noise would be a prerequisite to using this scheme.

D. Electronic Feedback

Similar to the all-optical feedback scheme, photon number squeezing can be performed with electronic feedback.[12] This technique was demonstrated using destructive detection of the signal laser field. In this scheme, the beam from a current-injection solid state diode laser is split into two components. The power in one component is converted to an electrical signal with a high quantum efficiency detector. This current signal is amplified, inverted, and summed into the injection current of the laser, as shown in Figure 12. The photon number in the feedback beam component is monitored by measuring the injection current at terminal (A). Readers familiar with lasers will recognize this scheme as that used to control the output of lasers equipped with 'light control' stabilization. This scheme is often used in ion and solid state lasers. The photon number in the other component beam is measured using a similar detector/amplifier circuit, terminal (B). Statistics of the difference in currents generated by the two detectors were also determined.

The results of these experiments are illustrated in the probability density plots of Figure 13. The Poisson probability for the free running laser is shown as the solid line on both the (A) and (B) terminal measurements. A reduction in the current, and thus photon number, variance is found in the signal used to control the laser output (Terminal A). On the other hand, the variance of the second beam is found to increase with feedback stabilization. In fact, by comparing these measurement statistics to those obtained with an LED, it was found that the photon statistics in the beam used for feedback were sub-Poisson and those of the other beam were super-Poisson, exhibiting a variance greater than $\langle n \rangle$. The statistics of the detector current difference is that of shot noise. This result is expected from discussions of the balanced detector given above. The bandwidth of the

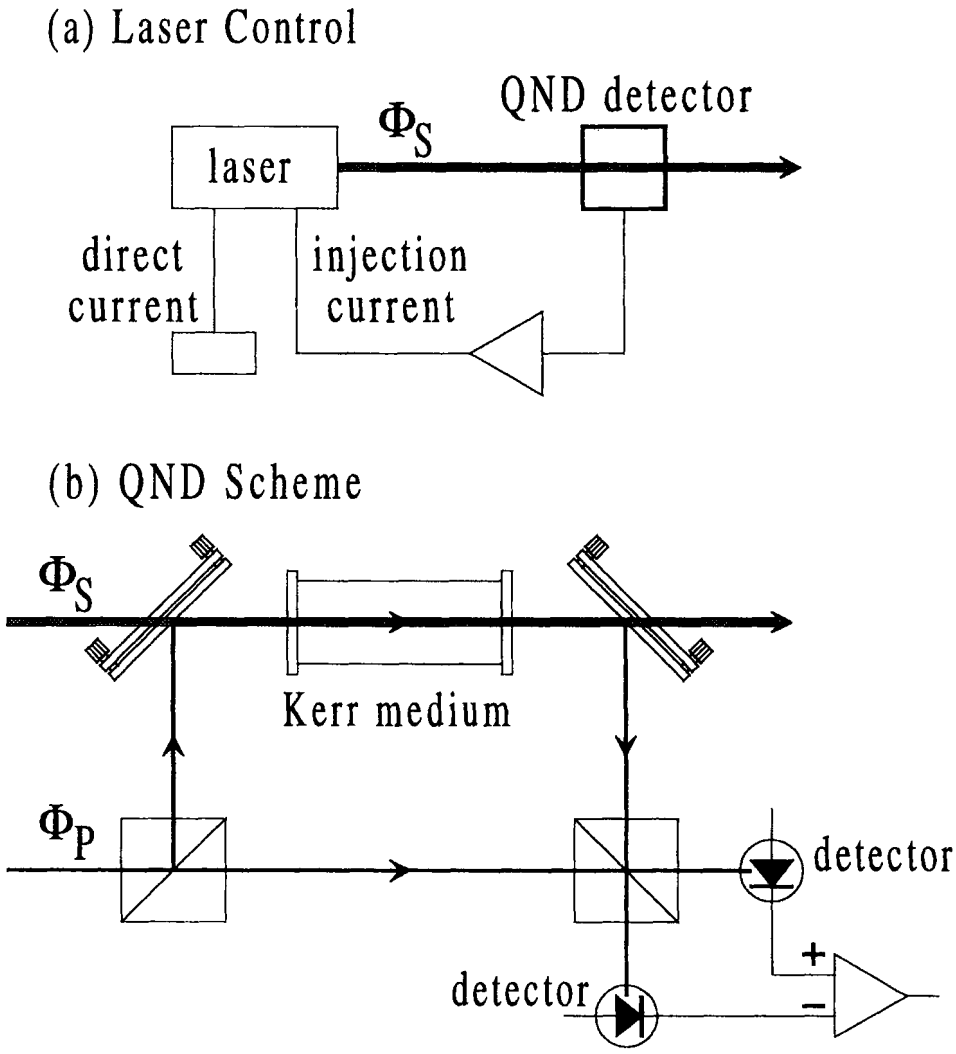

FIGURE 11. Use of the nonlinear Mach-Zehnder interferometer as a quantum nondemolition probe of the signal state. The signal laser produces a phase shift in the Kerr effect medium that is measured with the measurement beam. Results from the analysis of the measurement beam are subsequently used to control the signal beam through electronic feedback.

photon number squeezing was not as high as direct, all optical schemes. Maximum squeezing was 10 dB below the shot noise limit at around 2.5 MHz, decreasing to less than 5 dB at 20 MHz.

One may interpret the fact that the photon number variance in the beam used for feedback control was sub-Poisson, whereas that of the other beam was super-Poisson, as being a manifestation of the uncertainty principle. In particular, the phase uncertainty induced by increasing photon number certainty in one beam causes an increase in the photon number variance in the other beam. Although photon number squeezing was accomplished, the result is not of much consequence to measurement science because demolition detection was used. In fact, decreasing photon number variance in one beam increased that of the other. Moreover, these experiments showed that although electronic feedback stabilization may be useful in controlling excess noise in laser output, it does not result in sub-Poisson light generation. In

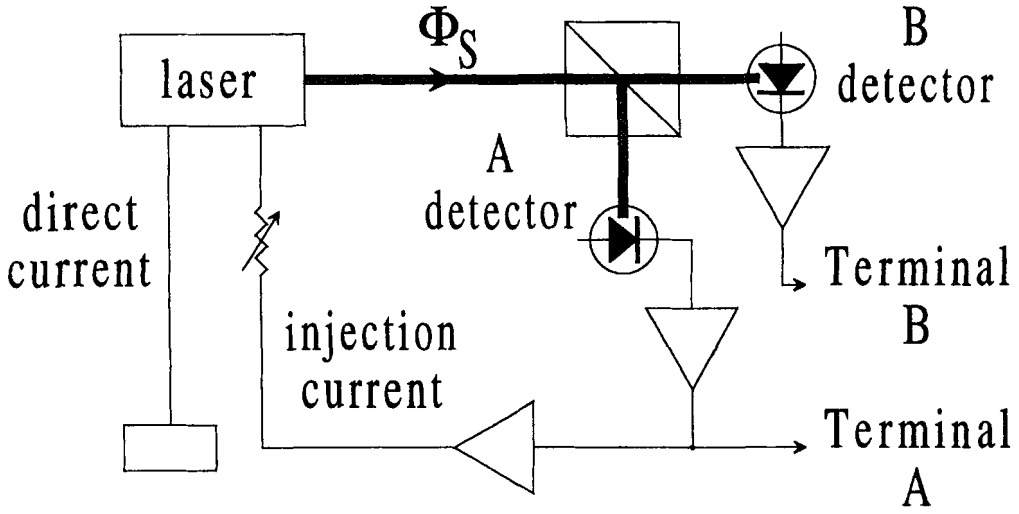

FIGURE 12. Use of a beamsplitter to directly sample the signal beam for electronic feedback control of a signal laser. The light power in both the signal and reference beams may be analyzed. However, only the reference beam is used to produce photon number squeezed states. This type of feedback is used in many commercial gas and solid-state lasers.

fact, the light produced in such a scheme is slightly super-Poisson.

E. Semiconductor Lasers

Yamamoto et al.[71,72] proposed that semiconductor laser driven by a high impedance constant current source produces photon number squeezed states through an internal feedback mechanism. The mechanism for this squeezing is not entirely understood.[73,74] However, experimental evidence suggests that a macroscopic coulomb blockade effect wherein the charge carrier density in optically active junction area is stabilized.[74] Essentially, the increased carrier density produced by passing current through the device produces a potential that, in turn, limits the current. As a consequence, the carrier density is stabilized in the active region. In the high quantum efficiency devices, for which squeezing is observed, the main carrier depletion mechanism is photon emission. With a high impedance constant current, the charge density is stabilized, which in turn stabilizes the photon emission rate. Each time a photon is emitted, the potential barrier decreases allowing the passage of another charge carrier. Along with the high impedance source, the coulomb blockade effect limits the current passing through the semiconductor gap to below that of the electron current shot noise. This is one example of limiting the rate of photon emission by controlling the rate process by which the photons are created.[9]

There are, in fact, many experimental observations of sub-Poisson light generation in semiconductor lasers.[74–83] The best experimental results to date have been obtained using a transverse junction stripe laser.[79] In the latter, photocurrent fluctuations were reported to be reduced by almost one order of magnitude, 8.3 dB below the shot noise limit (~85% noise suppression). Kitcheng et al.[83] obtained nearly a 4.0 dB reduction in noise below the shot noise limit using a commercially available index guided temperature-stabilized room temperature quantum well laser. This laser had 68% external quantum efficiency that is, 68% of the current resulted in photons leaving the laser. Degrada-

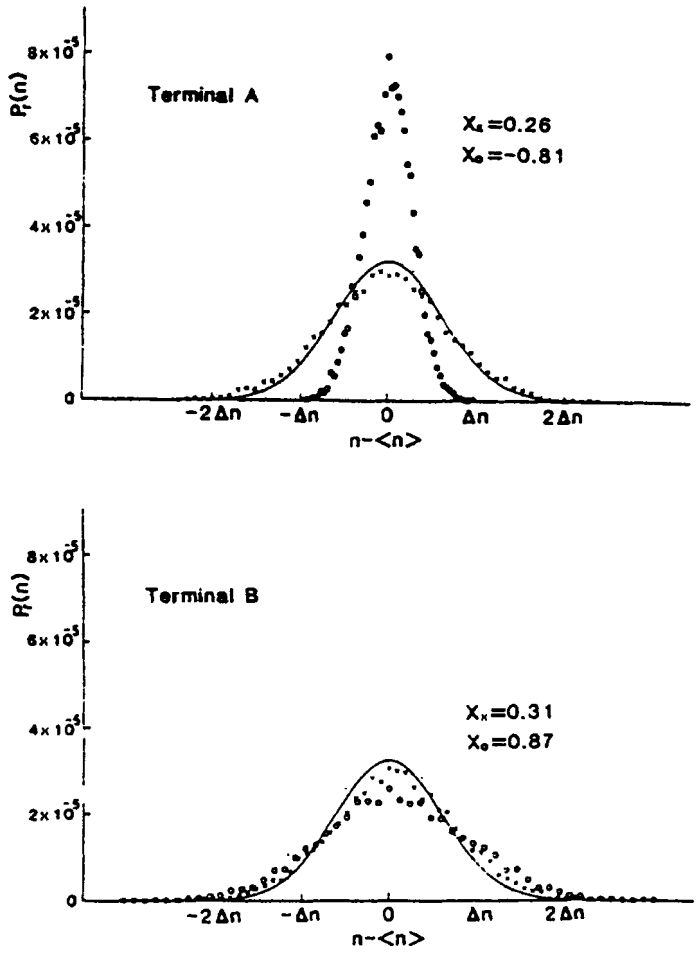

FIGURE 13. Probability density plots of signals produced using electronic feedback control experiments illustrated in Figure 12 with a diode laser source. A reduction in photon number variance is found in the sampled signal branch used to control laser output (Terminal A) as seen in the narrrower distribution of the stabilized (o) vs. free running (×) probability distributions. At the same time, the variance of the beam passing through the beamsplitter increases with feedback stabilization. The X values are second moments of the distributions, relative to that of the free-running laser. The relative second moments correspond to 7.2 dB squeezing in the controlled and 2.7 dB antisqueezing in the free branch, respectively. The Poisson distribution of the free running laser is shown as the solid line on both the (A) and (B). (Adapted from Yamamoto et al.[12] Figure 15.)

tion of the squeezing was found to occur at the onset of multimode operation. The photon number squeezed state bandwidth was limited to about 5 MHz.

The main problems with using laser diodes are the large amount of excess noise, mode instability, and high susceptibility to optical feedback-induced output fluctuation. It is not clear at this time whether sub-Poisson photon number emission can be obtained concurrently with controlled optical frequency and linewidth. A discussion of the relationship of excess $1/f$ optical noise in diode lasers to operating conditions and op-

tical bandwidth may be found in Reference 84. Discussions regarding characterization and control chaotic nature[85] of laser sources can be found in review publications.[86–88]

F. Sub-Poisson Emission from Light Emitting Diodes

Photon number squeezed light may also be produced in high quantum efficiency LEDs. LED sources are intrinsically less noisy than diode lasers. They do not suffer from excess noise due to multimode operation, mode jumping, and strong optical coupling to external reflective optics. Although the quantum efficiency of these devices is not thought to be as high as that of the diode laser, we have obtained encapsulated devices with as high as 36% external quantum efficiency at 836 nm from Hewlett-Packard. The main optical loss mechanisms in solid state emitters are light trapping through internal reflection and reabsorption by the AlGaAs. Both of these mechanisms are enhanced in the encapsulated devices because of the large refractive index mis-match between the AlGaAs semiconductor and the clear polymer encapsulating material. The external quantum efficiency of these devices can be further improved by matching the refractive index with multiple dielectric layers.

The first reported measurement of sub-Poisson light from a LED source was by Tapster et al.[89] The amount of noise reduction was small, ~0.2 dB, but the devices used had relatively low quantum efficiencies, 6 to 11% when operated at 194 K. The central emission wavelength of the diodes was about 950 nm. The initial report has been confirmed by several other researchers.[90–97] The best noise reduction obtained to date has been 1.4 dB below the shot noise limit, corresponding to a Fano factor of about 0.7.[92] The device used was a Hamamatsu model L2656 890 nm LED cooled to 77 K. The maximum external quantum efficiency for this LED was ~30%. However, when detector quantum efficiency is taken into account, the overall current-to-current quantum efficiency was only 12%.

Edwards[98] developed a semiempirical model to account for the photon noise suppression found in high quantum efficiency semiconductor laser and LEDs. The model and results are similar to those obtained by Yamamoto and co-workers.[73,97] At frequencies below those of the mean carrier lifetime prior to photon emission and the $1/RC$, the frequency response of the high-impedance current source driven LED, where R is the source impedance and C the capacitance of the LED, the current variance in the detector is

$$\sigma_d^2 = \eta^2\sigma_i^2 + \eta(1-\eta)\sigma_n^2 \qquad (59)$$

The current variance on the left-hand side, σ_d^2 is that of the photodetector used to measure the output of the semiconductor emitter. The quantum efficiency, α, is the total efficiency of the emission-detection process, $\eta = \eta_e\eta_d$. The two current variances on the right-hand side, σ_i^2 and σ_n^2, are that of the current passing though the junction and the recombination current within the junction, respectively. Carrier recombination is a Poisson process. For the high impedance constant current source, the recombination term dominates and the detector current variance becomes $\sigma_d^2 = \eta(1-\eta)\sigma_n^2$. Carrier recombination within the semiconductor results in the emission of a photon. Because the shot noise due to this process is proportional to the current flowing through the device, as is the photon emission, the Fano factor for photon detection is simply, $F = \sigma_d^2/\eta\sigma_n^2 = (1-\eta)$. This simple relationship has been confirmed for a number of measurements of LED emission. Fano factors less than one, and thus sub-Poisson statistics, are thus easily accomplished for high quantum efficiency devices with low losses between detector and emitter.

Of some interest in these devices is the correlations that can be obtained between two diode lasers or LEDs.[90–92] It has been know for some time that large correlations can exist between two or more light sources.[6,8] In particular, there is a large correlation between sum and difference frequency components produced by optically mixing two beams in a nonlinear medium or by simultaneous parametric up- and down-conversion. Correlation may also be obtained between signal and probe beams in the nondemolition detection scheme of Yamamoto et al.[12] and other twin-beam squeezing experiments.[49,99] Even without squeezing, correlations between two beams is similar in effect to squeezing in that detection of a photon in one beam indicated the presence of a photon in the other. For application to spectroscopy, correlations of this type may be more useful than simply reducing the noise in a single beam. The correlated photons may be used to enhance measurement precision because detection of a photon in one beam indicates the presence of a photon in the other. On the contrary, splitting an initially photon number squeezed beam at a beamsplitter produces negative correlation between photons detected at the two output ports. Although this negative correlation may also be used to reduce measurement errors, it is only practical if the initial photon number squeezed light does not have excess noise. Recall that there is no correlation between the simultaneous photon detection at the two output ports of a split classic coherent beam, except that due to excess source noise, and there is positive correlation between the photon detection events for thermal radiation.

An apparatus for measuring output correlation of two semiconductor emitters is shown in Figure 14.[90–92] The LEDs are driven by single high impedance, constant current source. Output from the two LEDs is measured simultaneously with the photodiodes and subsequently analyzed for correlation and relative noise. The coulomb blockade effect limits current through both devices connected to the high-impedance, constant current source. Wired in series, equal currents must pass through both LEDs. In this case the emission from the two sources can be highly correlated if either the quantum efficiencies are unity or the Fano factor for the driving current, F_e, is low. The driving current Fano factor, in turn, can be related to the apparatus parameters of series and LED shunt impedances. The normalized cross-correlation for the two emitter case is[91,92]

$$R_{1,2} = \frac{\eta F_e}{\eta F_e + (1-\eta)} \qquad (60)$$

A minimum driving current Fano factor of $F_e = 1/2$ occurs for circuits where the current source impedance is much higher than the shunt impedance of the LEDs.[91] In this case the two signals should exhibit a correlation of $R_{1,2} = \eta/[\eta + 2(1-\eta)]$ Note too that this equation predicts large correlations when the driving current is super-Poisson, that is, with current Fano factors $F_e \geq 1$, even when the LED quantum efficiency is low.

Kikuchi and Kakui[90] and Edwards and Pollard[91] independently reported on measured positive correlations in the photocurrents produced from the series circuit. In both cases it was found that the measured photodiode currents agreed with those predicted from the correlation equation.

Goobar et al.[92] also examined detector current correlations produced using a single current source to drive two high-efficiency LEDs. Their apparatus was designed to provide three types of driving currents, characterized by driving current Fano factors less than, equal to, and greater than unity. Shot noise limited current, thus a unit Fano factor was generated using a low-efficiency LED-photodiode pair as a current source. Sub-shot noise currents were produced with the high-impedance current source and super-

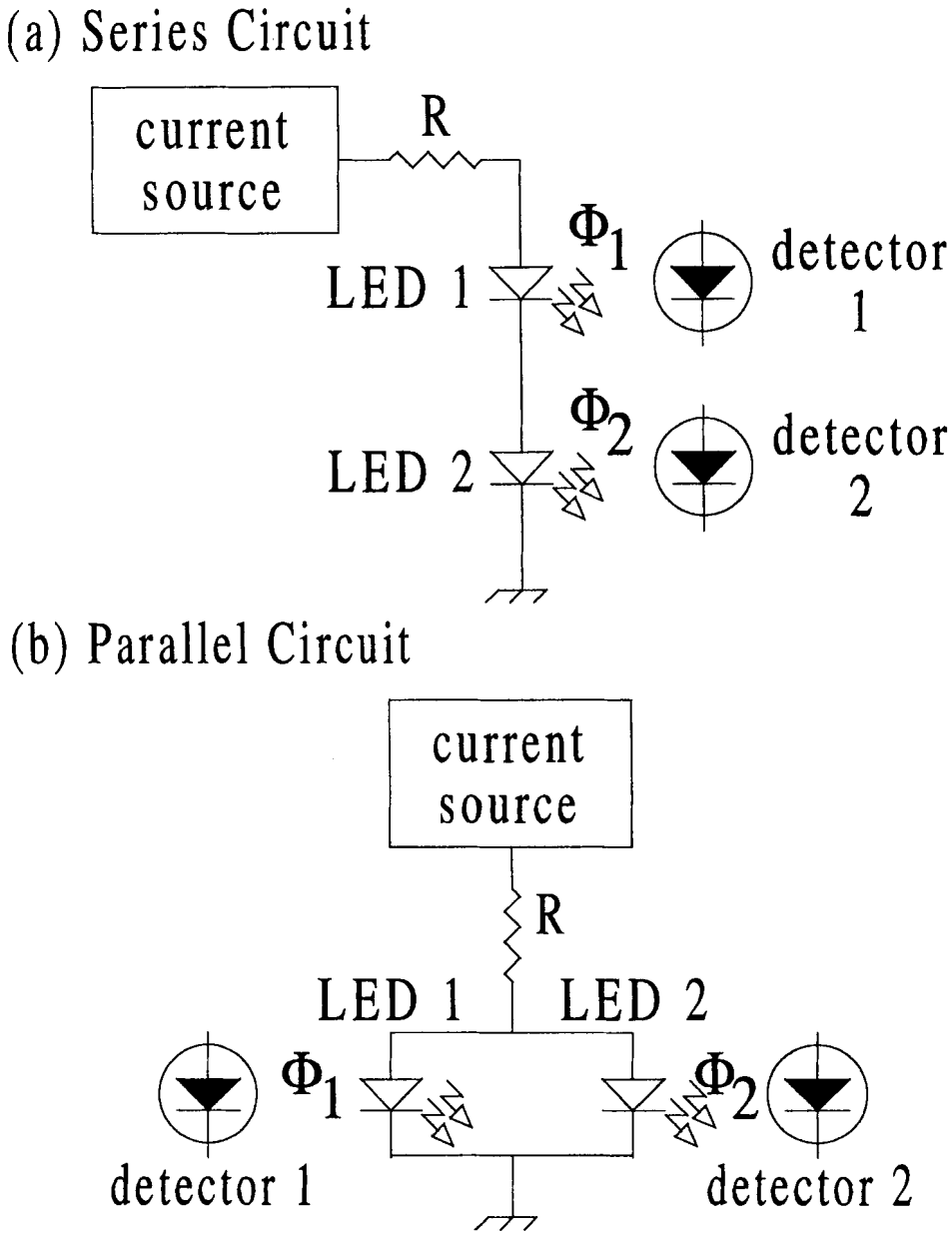

FIGURE 14. An apparatus for measuring squeezing and correlation in electronically coupled LED or diode lasers. A high-impedance, constant current source is used to drive the emitters. Correlations may be found in both the serial (A) and parallel (B) configurations.

Poisson currents were produced by using an oscillator-driven current source. Measurements were performed to determine the quantum efficiency and photon Fano factor. These parameters were subsequently used to determine the driving current Fano factor using the relationship, $F = \eta F_e(1-\eta)$. The electron current Fano factor was first deduced from a series of measurements on single LEDs. An electron current Fano factor of zero was found for the high-impedance current source. From this, the relative correlation predicted for the series LED measurements is predicted to be zero. Contrary to previous measurements,[90,91] their measurements confirm this prediction; no photocurrent correlation was found for

the parallel LEDs. It is difficult to assess why this discrepancy occurred. None of these references give adequate data regarding the electronic circuits used to drive the LED emitters to determine what, if any, differences exist. In addition, Goobar et al. use microwave attenuators to adjust the individual detector currents at the mixer/correlator. The attenuators were adjusted such that an attenuation of one detector equivalent to the quantum efficiency of the other channel was used to lower the differential current variance.[100–103]

Edwards and Pollard[91] and Goobar et al.[92] also measured correlations for the parallel configuration. Negative correlation coefficients are expected with parallel LEDs due to partitioning of electrons between the two LED circuit paths. Electron partitioning between the two circuit branches is similar to the photon partitioning that occurs at a beamsplitter.[73] Goobar et al. also found that the photocurrent variance was substantially lower for the parallel LED circuit than for the series circuit. Although this result is expected from the partition noise current model of Yamamoto and Haus,[73] it is not intuitively obvious why the photon fluctuations should be sub-Poisson when current partitioning between two diodes occurs.

G. Correlated Light

In a semiconductor laser, the output power, or photon production rate, is not linearly related to the electrical current due to changes in output coupling efficiency with optical mode, temperature, and other physical effects. The nonlinear effects tend to weaken correlations between electron current and output power. These effects do not occur in LEDs. Photon production in LEDs is linearly related to the current passing through the device. In fact, there is no reason why two LEDs must be used to examine the correlations. In a later publication than the initial electronic feedback photon number squeezed state generation,[12] Yamamoto and Haus[73] refined the model and point out that sub-shot-noise electrical current is not the source of sub-Poisson photon emission in the high impedance constant current-driven devices. In fact, the opposite cause and effect relationship probably exists. The self-regulating carrier density resulting from photon emission limits the electronic current through the device. Thus, the sub-Poisson photon emission process limits the current to sub-shot-noise variance levels. Because electrical current is limited by the photon emission process, there is no apparent reason why the electronic current cannot be used as a direct indicator of the photon flux being emitted from a high quantum-efficiency LED.

Correlations between single LED current[95] and diode laser current[103] and photodetector current have, in fact, been observed. In the LED experiments, difference currents below the shot noise limit were found using a system with a current-to-current quantum efficiency of $\eta \sim 0.27$. Correlations in the diode laser experiments, based on a single diode laser-photodetector pair, of nearly unit correlations were found over a bandwidth exceeding 1 GHz. Goobar et al.[93] used the fact that the photon production rate was highly correlated to the current to produce a photon amplifier that could, in principle, amplify photon number squeezed light. Their apparatus incorporated a number of LED-photodiode pairs (up to 8) connected in series. The current source for the LEDs was a single photodiode. The resulting circuit, termed an "optoelectronic photon number amplifier", could amplify electrical or photon currents while preserving the photon number squeezed aspect of the light on the LED current source detector. The apparatus was, of course, limited by the quantum efficiencies of the devices used to construct it. No net amplification was found for up to 8 LED-detector pairs. The total conversion electron current quantum efficiency was

~0.77. Correlation between currents passing through the LED array and the photodetector currents was high, judging from the substantially reduced differential noise current.

It has been shown that light can be electro-optically amplified with little additional noise, thus preserving any sub-Poisson character of the input signal. Amplification using photons should be intrinsically less susceptible to producing excess flicker noise because, compared with electrons,[104] photons are only weakly scattered. Electro-optical-based amplifiers may be designed that could provide relatively noise-free amplification of either electron or photon currents. In fact, Cheung and Edwards reported recently on the design of an electro-optical based current amplifier with positive feedback. Although the design was not implemented, computer modeling showed that the design could give a current gain of 14.7 dB, with a noise figure of 1.5 dB.[105]

H. Other Means to Produce Squeezed Light

Photon number-phase squeezed light can also be produced by the conversion or passage of coherent or chaotic light in a nonlinear medium. It has been known for some time that multiphoton interactions can produce squeezed states.[7,106] Mandel predicted that squeezed states would be obtained in second-harmonic generation.[107] Squeezing through second harmonic generation has been observed by a number of researchers.[108-110] Experimental realization of substantial squeezing was recently attained and theoretically modeled.[60] These experiments, a monolithic standing wave doubler (cavity device) is used to produce the second harmonic of the Nd:YAG excitation laser. The second harmonic light was analyzed with a balanced mixer. Approximately 0.75 dB of squeezing was observed over a bandwidth of about 60 MHz. The high-frequency roll off of the squeezed light was due to the doubler cavity. Roll off at the low-frequency end was due to excess noise in the excitation laser. These results were reported to fit well the theory for this type of squeezing. Extrapolating squeezing to the lower frequencies hidden by excess noise revealed over 3 dB of squeezing. As found in most laser sources, the excess noise obscures the attempts to produce highly squeezed light.

Photon number squeezed states may also be obtained directly from a laser source when the output coupling, excitation rate, and relaxation rates are within certain bounds. This is essentially a means to produce squeezed light through "optical feedback". Ralph and Savage theoretically examined squeezing in conventionally pumped three- and four-level lasers.[111] As was the case for semiconductor diode lasers, squeezed light might already be produced in conventional lasers such as the helium-neon. The authors point out that this fact may have escaped notice because measurements of the output statistics of helium neon lasers were made using photomultiplier tube detection of the attenuated output beam.

VIII. CONCLUSION

Little has changed in terms of applications since the 1988 *Analytical Chemistry* focus report introduced the concept of squeezed light to the analytical chemist.[112] Although several papers mention the possibility of high-precision optical measurements, there are few, if any, practical working examples.[113-116] No disrespect for the focus report intended. However, the prediction that scientists would "propose novel squeezed-light applications" has just not come true. This is probably because emphasis has changed from measurement accuracy to nano-measurement and other new regimes. Squeezed light was dismissed because generation required costly hardware while pro-

ducing only marginally quadrature squeezed light. Although sub-Poisson, quadrature squeezed light was of little benefit to persons not performing interferometric measurements. Even there, the costs outweigh the benefits when one million dollars is required to make a measurement that is only an order of magnitude better than that which can be obtained with equipment costing only a few tens of thousands.

However, much has changed in the electronics and electro-optics industries in the last 8 years. Semiconductor detectors with quantum efficiencies and noise figures exceeding those of the photomultiplier tube are now available for few dollars, as are high quantum efficiency light emitting diodes and semiconductor lasers and low-noise electronic components. Coupled with ultra-low-noise optical detection schemes,[117] the relative ease at which squeezed light can be generated using semiconductor devices could find application in analytical spectroscopy. One may presently assemble an optical absorption apparatus based on squeezed LEDs for about $100. The problem of the red wavelengths is currently being resolved with the "blue light" LEDs and diode lasers.[118] Regardless of whether background absorption, scattering, and reflection losses are present, the accuracy of any optical absorption measurement is limited by the precision of the optical measurement. The attainable precision is currently below what was thought to be the ultimate limit — that due to shot noise. The question of application of these sub-Poisson light sources to optical spectroscopy does not appear to be one of practicality or financial burden. However, analytical chemists that attempt to keep up with new methods in analysis have little time to do the same in optical physics and electro-optics engineering. Instead, we look to commercial development to keep abreast of the current technology. However, analytical instrumentation has apparently fallen behind in terms of new electro-optics technology, which has been primarily geared toward optical communications and consumer products. One is hard pressed to find commercial spectrometer instrumentation based on the traditional LED light source, let alone a sub-Poisson spectrometer.

One of the surprising consequences of generation and detection of squeezed light has been in furthering the understanding of fundamental noise sources in electronic circuits. By measuring photon number squeezed states with noise less than the shot noise limit using semiconductor photodiode detectors, it has been inadvertently demonstrated that the Shottky noise, that is, current variance produced by the passage of electrons across a barrier, is not intrinsic to the transport of electrons in a conductor. This may seem contrary to the fundamental physics of transport. However, one basic assumption used for deriving the binomial and subsequent Poisson probability distributions is that the objects do not interact. In fact, electrons interact though a space-charge effect. It has been known for some time that this interaction results in sub-Poisson current variance in thermionic vacuum diodes.[63] It is not unreasonable that electron transport through conductors and even semiconductors may exhibit similar noise-suppression effects.

It is difficult to assess what is on the horizon. Simple, inexpensive technology for squeezed generation is currently available at the local electronics supply houses. The technology apparently awaits testing and application. The main question is if chemical analysis is a follower or a leader in technology application.

REFERENCES

1. Einstein, A. *Z. Physik.* **1909** *10,* 185.
2. Mandel, L.; Wolf, E. *Selected Papers on Coherence and Fluctuations of Light (1850-1966).* **MS 19** SPIE Optical Engineering Press, Bellingham, WA, 1990.

3. Mandel, L.; Wolf, E. *Rev. Mod. Phys.* **1965,** *37,* 231.

4. Dicke, R. H. *Phys. Rev.* **1953** *93,* 99.

5. Steinfeld, J. I. *Molecules and Radiation.* 2nd ed.; MIT Press Cambridge, MA, 1986.

6. Yariv, A. *Quantum Electronics,* 3rd ed., Wiley, NY, 1989.

7. Peřina, J. *Photon Statistics and Coherence in Nonlinear Optics,* **MS 39,** SPIE Optical Engineering Press, Bellingham, WA, 1991.

8. Mandel, L.; Wolf, E. *Optical Coherence and Quantum Optics,* Cambridge University Press, New York, 1995.

9. Teich, M. C.; Saleh, B. E. A. *Photon Bunching and Antibunching,* in *Progress in Optics, Vol. XXVI,* E. Wolf, ed., Elsevier, 1988.

10. Caves, C. M. *Phys Rev. D.* **1981,** *23,* 1693.

11. Walls, D. F. *Nature,* **1983,** *306,* 141.

12. Yamamoto, Y.; Imoto, N.; Machida, S. *Phys. Rev. A.* **1986,** *33,* 3243.

13. Hanbury Brown, R.; Twiss, R. Q. *Nature.* **1956,** *177,* 27.

14. Hanbury Brown, R.; Twiss, R. Q. *Proc. R. Soc. A.* **1957,** *242,* 300.

15. Hanbury Brown, R.; Twiss, R. Q. *Proc. R. Soc. A.* **1957,** *243,* 291.

16. Morgan, B. L.; Mandel, L. *Phys. Rev. Lett.* **1966,** *16,* 1012.

17. Papoulis, A. *Probability, Random Variables, and Stochastic Processes,* 2nd ed., McGraw-Hill, NY, 1984.

18. Freed, C; Haus, H. A. *IEEE J. Quant. Electron.* **1966,** *QE-2,* 190.

19. Martienssen, W.; Spiller, E. *Phys. Rev. Lett.* **1966,** *16,* 531.

20. Glauber, R. J. *Phys. Rev.* **131,** 2766, **1963.**

21. Sudarshan, E. C. G. *Phys. Rev. Lett.* **1963,** *10,* 277.

22. Titulaer, U. M.; Glauber, R. J. *Phys. Rev.* **1966,** *145,* 1041.

23. Mollow, B. R.; Glauber, R. J. *Phys. Rev.* **1966,** *160,* 1076.

24.. Mollow, B. R.; Glauber, R. J. *Phys. Rev.* **1966,** *160,* 1097.

25. Yuen, H. P. *Phys. Rev. A.* **1976,** *13,* 2226.

26. Peřina, J.; Bajer, J. *Phys Rev. A.* **1990,** *41,* 516.

27. Stoler, D. *Phys. Rev. D.* **1970,** *1,* 3217.

28. Hollenhorst, J. N. *Phys. Rev. D.* **1971,** *19,* 1669.

29. Bondurant, R.; Shapiro, J. H. *Phys. Rev. D.* **1984,** *30,* 2548.

30. Schleich, W.; Wheeler, J. A. *J. Opt. Soc. Am. B.* **1987,** *4,* 1715.

31. Mandel, L. *Phys. Rev. Lett.* **1982,** *49,* 136.

32. Mandel, L. *Opt. Comm.* **1982,** *42,* 437.

33. Peřina, J.; Peřinová, V.; Kodousek, J. *Opt. Comm.* **1984,** *49,* 210.

34. Kitagawa, M.; Yamamoto *Phys. Rev. A.* **1986,** *34,* 3974.

35. Reid, M. D.; Walls, D. F. *Phys. Rev. A.* **1985,** *31,* 1622.

36. Slusher, R. E.; Hollberg, L. W.; Yurke, B.; Mertz, J. C.; Valley, J. F. *Phys. Rev. Lett.* **1985,** *55,* 2409.

37. Slusher, R. E.; Yurke, B.; Hollberg, L. W.; Mertz, J. C. *J. Opt. Soc. Am. A.* **1985,** *2,* 107.

38. Raymer, M. G.; Rzazewski, K.; Mostowski, J. *Opt. Lett.* **1982,** *7,* 71.

39. Walmsley, I. A.; Raymer, M. G. *Phys. Rev. Lett.* **1983,** *50,* 962.

40. Raymer, M. G.; Mostowski, J. *Phys. Rev. A.* **1981,** *24,* 1980.

41. Wu, L.-A.; Kimble, H. J.; Hall, J. L.; Wu, H. *Phys. Rev. Lett.* **1986,** *57,* 691.

42. Xiao, M.; Wu, L.-A.; Kimble, H. J. *Phys. Rev. Lett.* **1987,** *41,* 413.

43. Wu, L.-A.; Xiao, M.; Kimble, H. J. *J. Opt. Soc. Am. B.* **1987,** *4* ,1465.

44. Xiao, M.; Wu, L.-A.; Kimble, H. J. *Opt. Lett.* **1988,** *13,* 476.

45. Breitenbach, G., Müller, T.; Pereira, S. F.; Poizat, J.-Ph.; Schiller, S.; Mlynek, J. *J. Opt. Soc. Am. B.* **1995,** *12,* 2304.

46. Mertz, J.; Debuisschert, T.; Heidmann, A.; Fabre, C.; Giacobino, E. *Opt. Lett.* **1991,** *16,* 1234.

47. Leong, K. W.; Wong, N. C.; Shapiro, J. H. *Opt. Lett.* **1990,** *15,* 1058.

48. Kimble, H. J. *Phys. Rep.* **1992,** *219,* 227.

49. Heidmann, A.; Horowicz, R. J; Reynaud, S.; Giacobino, E. Fabre, C.; Camy, G. *Phys. Rev. Lett.* **1987,** *59,* 2555.

50. Orozco, L. A.; Raizen, M. G., Xiao, M.; Brecha, R. J.; Kimble, H. J. *J. Opt. Soc. Am. B.* **1987,** *4,* 1490.

51. Grangier, P.; Slusher, R. E.; Yurke, B.; LaPorta, A. *Phys. Rev. Lett.* **1987,** *59,* 2153.

52. Fox, A. M.; Baumberg, J. J.; Dabbicco, M.; Hunter, B.; Ryan, J. F. *Phys. Rev. Lett.* **1995,** *74,* 1728.

53. Shelby, R. M.; Levenson, M. D.; Perlmutter, S. H.; DeVoe, R. G.; Walls, D. F. *Phys. Rev. Lett.* **1986,** *57,* 691.

54. Haus, H. A. *J. Opt. Soc. Am. B.* **1995,** *12,* 2019.

55. Levenson, M. D.; Shelby, R. M. *J. Mod. Opt.* **1987,** *34,* 775.

56. Wong, N. C.; Leong, K. W.; Shapiro, J. H. *Opt. Lett.* **1990,** *15,* 891.

57. Yariv, A. *Optical Electronics,* 3rd ed., Holt, Rinehart and Winston, New York, 1985.

58. Haus, H. A. *J. Opt. Soc. Am. B.* **1995,** *12,* 2019.

59. Wu, L.-A.; Xiao, M.; Kimble, H. J. *J. Opt. Soc. Am. B.* **1987,** *4,* 1465.

60. Ralph, T. C.; Taubman, M. S.; White, A. G.; McClelland, D. E.; Bachor, H.-A. *Opt. Lett.* **1995,** *20,* 1316.

61. Bachor, H.-A.; Fisk, P. T. H. *Appl. Phys. B.* **1989,** *49,* 291.

62. Bacon, A. M.; Zhao, H. Z.; Wang, L. J.; Thomas, J. E. *Appl. Opt.* **1995,** *34,* 5326.

63. Smullin., L. D.; Haus, H. A. *Noise in Electron Devices,* John Wiley, New York, 1959.

64. van der Ziel, A. *Noise in Solid State Devices and Circuits,* John Wiley, New York, 1985.

65. Poularikas, A. D.; Seely, S. *Signals and Systems,* PWS Engineering, Boston, MA, 1985.

66. Maeda, M. W.; Kumar, P.; Shapiro, J. H. *Opt. Lett.* **1987,** *12,* 161.

67. Machida, S.; Yamamoto, Y. *Opt. Lett.* **1989,** *14,* 1045.

68. Vogel, K.; Risken, H. *Phys. Rev. A.* **1989,** *49,* 2857.

69. Smithey, D. T.; Beck, M.; Raymer, M. G.; Faridani, A. *Phys. Rev. Lett.* **1993,** *70,* 1244.

70. Carruthers, P.; Neito, M. M. *Rev. Mod. Phys.* **1968,** *40,* 411.

71. Yamamoto, Y.; Machida, S.; Nilsson, O. *Phys. Rev. A.* **1986,** *34,* 4025.

72. Yamamoto, Y.; Machida, S. *Phys. Rev. A.* **1987,** *35,* 5114.

73. Yamamoto, Y.; Haus, H. A. *Phys. Rev. A.* **1992,** *45,* 6596.

74. Kim, J.; Kan, H.; Yamamoto, Y. *Phys. Rev. B.* **1995,** *52,* 2008.

75. Machida, S.; Yamamoto, Y.; Itaya, Y. *Phys. Rev. Lett.* **1987,** *58,* 1000.

76. Machida, S.; Yamamoto, Y. *Phys. Rev. Lett.* **1988,** *60,* 792.

77. Machida, S.; Yamamoto, Y. *Opt. Lett.* **1989,** *14,* 1045.

78. Richardson, W. H.; Shelby, R. M. *Phys. Rev. Lett.* **1990,** *64,* 400.

79. Richardson, W. H.; Machida, S.; Yamamoto, Y. *Phys. Rev. Lett.* **1991,** *66,* 2867.

80. Freeman, M. J.; Wang, H.; Steel, D. G.; Craig, R.; Scifres, D. R. *Opt. Lett.* **1993,** *18,* 379.

81. Freeman, M. J.; Wang, H.; Steel, D. G.; Craig, R.; Scifres, D. R. *Opt. Lett.* **1993,** *18,* 2141.

82. Kitching, J.; Yariv, A.; Shelvy, Y. *Phys. Rev. Lett.* **1995,** *74,* 3371.

83. Kitching, J.; Provenzano, D.; Yariv, A. *Opt. Lett.* **1995,** *20,* 2526.

84. Fronen, R. J. *IEEE J. Quant. Electron.* **1990,** 26, 1742.

85. *Order and Chaos in Nonlinear Physical Systems,* Lundqvist, S., March, N. H., Tosi, M., Eds., Plenum, New York, 1988.

86. *Laser Noise,* Roy, R., Ed., Vol. 1376, SPIE Proceedings, 1991.

87. *Chaos in Optics,* Roy, R., Ed., Vol. 2039, SPIE Proceedings, 1993.

88. Roy, R.; Gills, Z.; Thornburg, K. S. *Optics and Photon News.* **1994**, *5*(7), 8.

89. Tapster, P. R.; Rarity, J. G.; Satchell, J. S. *Europhys. Lett.* **1987**, *4*, 293.

90. Kikuchi, K.; Kakui, M. *IEEE Quant. Electron. Lett.* **1992**, *28*, 1626.

91. Edwards, P. J.; Pollard, G. H. *Phys. Rev. Lett.* **1992**, *69*, 1757.

92. Goobar, E.; Karlsson, A.; Björk, G.; Rigole, P.-J. *Phys. Rev. Lett.* **1993**, *70*, 437.

93. Goobar, E.; Karlsson, A.; Björk, G.; Nilsson, O. *Opt. Lett.* **1993**, *18*, 2138; **1994**, *19*, 922.

94. Roch, J.-F.; Poizat, J. P.; Grangier, P. *Phys. Rev. Lett.* **1993**, *71*, 2006.

95. Goobar, E.; Karlsson, A.; Björk, G. *Phys. Rev. Lett.* **1993**, *71*, 2002.

96. Hirano, T.; Kuga, T. *IEEE J. Quant. Electron.* **1995**, *31*, 2236.

97. Kim, J.; Kan, H.; Yamamoto, Y. *Phys. Rev. B.* **1995**, *52*, 2008.

98. Edwards, P. J. *IEEE J. Quant. Electron.* **1993**, *29*, 2302.

99. LaPorta, A.; Slusher, R. E.; Yurke, B. *Phys. Rev. Lett.* **1989**, *62*, 28.

100. Karlsson, A.; Björk, G. *Phys. Rev. A.* **1991**, *44*, 7669.

101. Mertz, J.; Heidmann, A.; Fabre, C. *Phys. Rev. A.* **1991**, *44*, 3229.

102. Bachor, H-.A.; Rottengarter, P.; Savage, C. M. *Appl. Phys. B.* **1992**, *55*, 258.

103. Goobar, E.; Karlsson, A.; Machida, S. *IEEE J. Quant. Electron.* **1993**, *29*, 386.

104. Handel, P. H. *IEEE Trans. Electron. Dev.* **1994**, *41*, 2023.

105. Cheung, W. N.; Edwards, P. J. *IEEE J. Quant. Electron.* **1996**, *32*, 502.

106. Voigt, H.; Bandilla, A.; Ritze, H.-H. *Z. Physik B.* **1980**, *36*, 295.

107. Mandel, L. *Opt. Comm.* **1982**, *42*, 437.

108. Sizmann, A.; Horowicz, R. J.; Wagner, G.; Leuchs, G. *Opt. Comm.* **1990**, *80*, 138.

109. Kürz, P.; Paschotta, R.; Fiedler, K.; Mlynek, J. *Europhys. Lett.* **1993**, *24*, 449.

110. Paschotta, R.; Collett, M.; Kürz, P.; Fiedler, K.; Bachor, H.-A.; Mlynek, J. *Phys. Rev. Lett.* **1994**, *72*, 3807.

111. Ralph, T. C.; Savage, C. M. *Opt. Lett.* **1991**, *16*, 1113.

112. Cunningham, D. *Anal. Chem.* **1988**, *60*, 343A.

113. Xiao, M.; Wu, L.-A.; Kimble, H. J. *Opt. Lett.* **1988**, *13*, 476.

114. Polzik, E. S.; Carri, J.; Kimble, H. J. *Phys. Rev. Lett.* **1992**, *68*, 3020.

115. Polzik, E. S.; Carri, J.; Kimble, H. J. *Appl. Phys. B.* **1992**, *55*, 279.

116. Inoue, S.; Björk, G.; Yamamoto, Y. *SPIE Proceedings on Laser Frequency Stabilization and Noise Reduction.* **1995**, *2378*, 99.

117. Haller, K. L.; Hobbs, P. C. D. *SPIE Proceeding on Optical Methods for Ultrasensitive Detection and Analysis: Techniques and Applications.* **1991**, *1435*, 298.

118. Levi, B. G. *Physics Today.* **1996**, *49*(4), 18.